OECD/MCCI-2009-TR04

OECD MCCI Project
Small-Scale Water Ingression and Crust Strength Tests (SSWICS)
SSWICS-12 Test Data Report: Thermal HydraulicResults

Rev. 2 - FINAL

September, 2009

by:

S. Lomperski, A. Ramirez, M. T. Farmer, D. Kilsdonk, R. Aeschlimann

Nuclear Engineering Division
Argonne National Laboratory
9700 S. Cass Avenue
Argonne, IL 60439
USA

Table of Contents

1. Introduction 1
2. System Description 2
2.1 General 2
2.2 Injection Supply System 2
2.3 Injection Nozzles 6
3. Data Acquisition and Control Systems 8
3.1 Instrumentation 8
3.1 General 11
4. Test Parameters and Course of Test 12
5. Sensor Malfunctions and Abnormalities 14
6. Data Reduction 14
7. Post Test Exams 16

List of Plots

A.1 Temperatures in tungsten thermowell; north melt quadrant 22
A.2 Temperatures in tungsten thermowell; south melt quadrant. 22
A.3 Temperatures in tungsten thermowell; east melt quadrant 23
A.4 Temperatures in tungsten thermowell; west melt quadrant 23
A.5 Temperatures of selected steel structures. 24
A.6 Total pressure in reaction vessel and position of valve V-quench 24
A.7 Condensate tank inventory as measured by ΔP and level sensors 25
A.8 Condensate tank liquid inventory 25
A.9 HX secondary side flow rate and water injection valve position 26
A.10 Secondary side fluid temperatures at HX inlet and outlet 26
A.11 Miscellaneous gas and fluid temperatures 27
A.12 Fluid temperatures in the condensate tank 27
A.13 Gauge pressure measured by reservoir level sensors 28
A.14 Heat flux as measured through condensate tank levels and HX heat load 28

1. Introduction

The Melt Attack and Coolability Experiments (MACE) program at Argonne National Laboratory addressed the issue of the ability of water to cool and thermally stabilize a molten core/concrete interaction (MCCI) when the reactants are flooded from above. These experiments provided unique, and for the most part repeatable, indications of heat transfer mechanisms that could provide long term debris cooling. The tests provided data regarding the nature of corium interactions with concrete, the heat transfer rates from the melt to the overlying water pool, and the role of noncondensable gases in the mixing processes that contribute to melt quenching. However, due to the integral nature of the tests, several questions regarding the crust freezing behavior could not be adequately resolved. These questions include:

- To what extent does water ingression into the crust increase the melt quench rate above the conduction-limited rate and how is this affected by melt composition and system pressure?
- What is the fracture strength of the corium crust when subjected to a particular thermal-mechanical load and how does it depend upon the melt composition?

A series of separate-effects experiments was carried out during the MCCI-1 program to address these issues. A test apparatus denoted SSWICS (Small Scale Water Ingression and Crust Strength) was constructed and used to quench ϕ30 x 15 cm deep melts at atmospheric pressure and also at 4 bar. The data indicated that the rate of cooling associated with water ingression, which occurs via cracks induced by thermal stresses, decreases with increasing melt concrete content. In addition, the cooling rate was shown to be insensitive to concrete type and system pressure. Companion experiments determined the strength of the ingots produced by these quench tests and it was found that the extensive cracking within the corium made the material structurally weak and that strength is essentially independent of corium composition over the tested composition range.

The SSWICS tests for the MCCI-1 program were generic in nature and were intended to validate water ingression models that predict ex-vessel corium cooling rates. Data was also generated to validate structural models used to predict the strength of corium crusts. The test described in this report, SSWICS-12, differs from those of the previous program in that it is intended to demonstrate the performance characteristics of a particular type of engineered corium cooling system. The system is designed to inject water into the corium from below to enhance the cooling rate far beyond that achievable by top flooding alone.

SSWICS-12 is similar in many respects to the preceding tests, e.g., fully oxidized melt with concrete constituents, 30 cm melt diameter, inert basemat, quench at 1 bar, and condensation of steam with collection of the condensate to measure gross cooling rate. The major departure from previous tests is the addition of water injection nozzles cast within the basemat. Each injection line has its own water supply and flow rate sensor. The melt is partitioned into quadrants using metal plates to create, in effect, four independent and simultaneous injection tests. Each nozzle has a different driving head. The purpose of this experiment is to determine the following:

- the minimum driving head required to ensure water injection into the melt
- the water flow rate to each nozzle
- the cooling rate of each melt quadrant
- the effect of water injection on crust morphology

The melt depth is 30 cm (versus 15 cm for all previous tests) so that it is closer to the 20-30 cm depth expected in a plant. This report includes a description of the test apparatus, the instrumentation, plots of the recorded data, and some rudimentary data reduction.

2. System Description

2.1 General

The SSWICS reaction vessel (RV) has been designed to hold at least 100 kg of melt at an initial temperature of 2500°C. The RV lower plenum consists of a 67.3 cm long, 45.7 cm outer diameter carbon steel pipe (Fig. 2.1). The pipe is insulated from the melt by a 6.4 cm thick annulus of cast MgO that is denoted the "liner". The selected pipe and insulation dimensions result in a melt diameter of 30 cm and a surface area of 707 cm^2. The melt depth for a typical corium charge of 75 kg is about 15 cm. The RV lower flange is insulated with a 6.4 cm thick slab of cast MgO (the "basemat") that spans the entire inner diameter of the pipe. The basemat and liner form the crucible that holds the corium.

The RV upper plenum consists of a second section of pipe with a stainless steel protective liner. Three 10 cm pipes welded near the top of the vessel provide 1) a vent line for the initial surge of hot noncondensable gases generated by the thermite reaction, 2) a pressure relief line with a rupture disk (7.7 bar at 100°C), and 3) an instrument flange for the absolute pressure transmitter that measures the reaction vessel pressure. A baffle is mounted below the upper flange prevents water droplets from being carried up towards the condenser, which would adversely affect the heat flux measurement. A fourth 10 cm pipe welded to the top flange provides an outlet to carry steam from the quenching melt to four cooling coils. The water-cooled coils condense the steam, which is collected within a 200 cm high, 20 cm diameter condensate tank (CT). Fig. 2.3 gives an overview of the entire SSWICS melt-quench facility.

The corium is divided into quadrants by 10 mm thick tungsten plates. The partitions have machined slots so that one fits over the other in an interlocking cruciform. They are supported by 20 mm deep grooves in the liner to discourage shifting under lateral loads. The partition consists of two stacked sections, each with a height of 20 cm, creating a 40 cm high wall within the melt. Figure 2.2 provides a detailed view of the lower plenum and basemat including the tungsten partitions.

2.2 Injection Supply System

Four 36-liter tanks provide independent reservoirs to supply the nozzles with water. The nozzles are gravity fed and so the driving pressure for injection is set by the elevation difference between the nozzle and the tank water level (Fig. 2.4). A check valve in each line prevents back flow up into the tank and isolation valves are opened when the RV preheat phase of the test begins.

The tanks are positioned at different levels to generate the desired range of driving pressures. A pressure equalization line links the RV gas space to the gas spaces of all four tanks, ensuring that the driving head for the nozzles is set only by the nozzle/tank elevation difference. This is necessary because the RV pressure spikes for a short period following initial water injection. If the reservoirs are not at the absolute pressure of the RV, the initial pressure spike will halt water injection, causing steam production and RV pressure to drop, which in turn permits continued water injection. It is likely that the system would oscillate during the early period of the test.

The tanks are positioned to provide initial net driving heads of 0.05, 0.1, 0.15, and 0.2 bar. The net driving head ΔP is defined here as the head remaining after subtracting the hydrostatic head associated with the melt:

$$\Delta P = \rho_l g L - \rho g h \big|_{corium}$$

where h is the height of the corium, 30 cm for this test, L is the distance from the bottom of the corium pool to the tank water surface, and ρ_l and ρ are the coolant and corium densities, respectively. The head

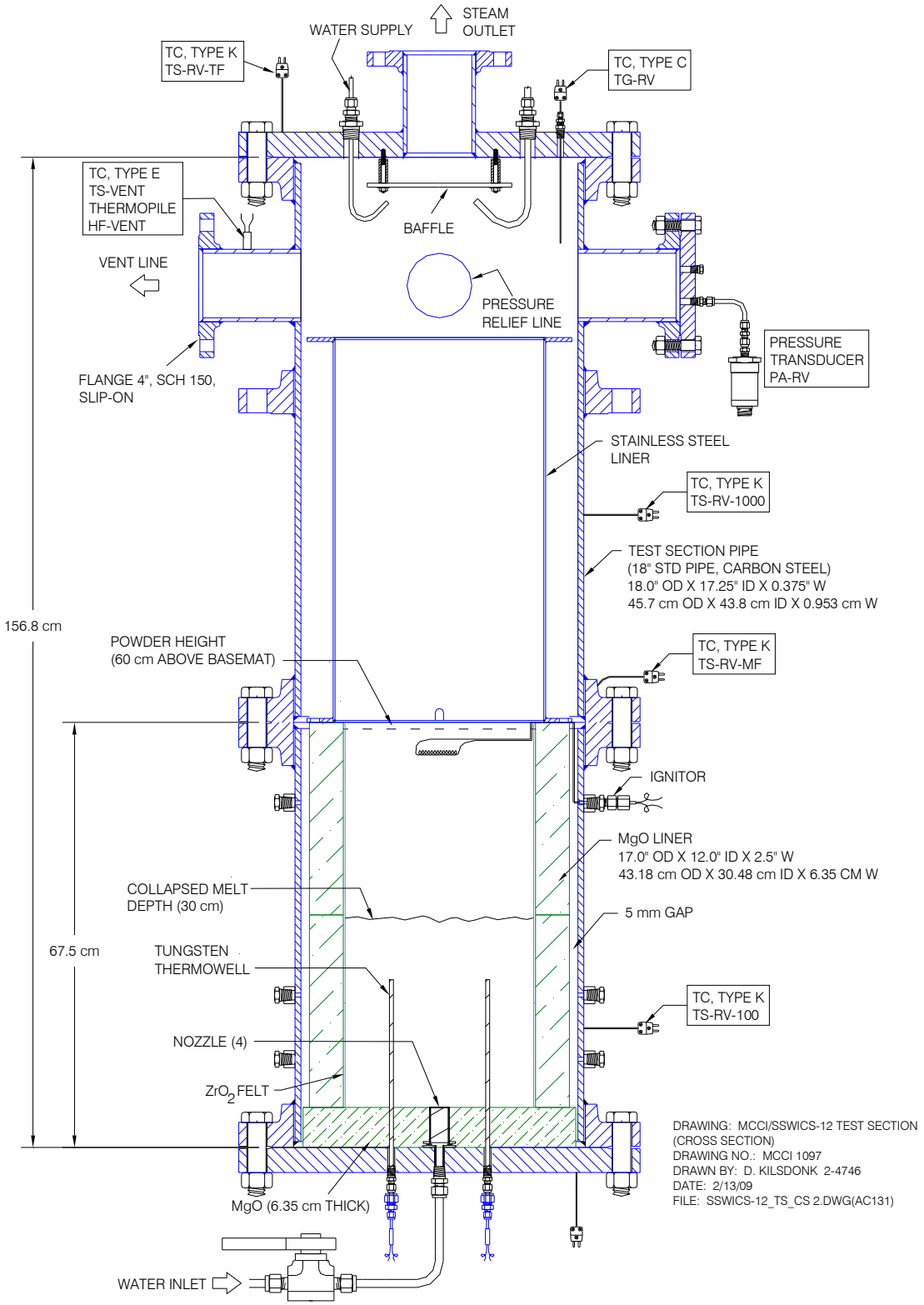

Figure 2.1. Side view of reaction vessel.

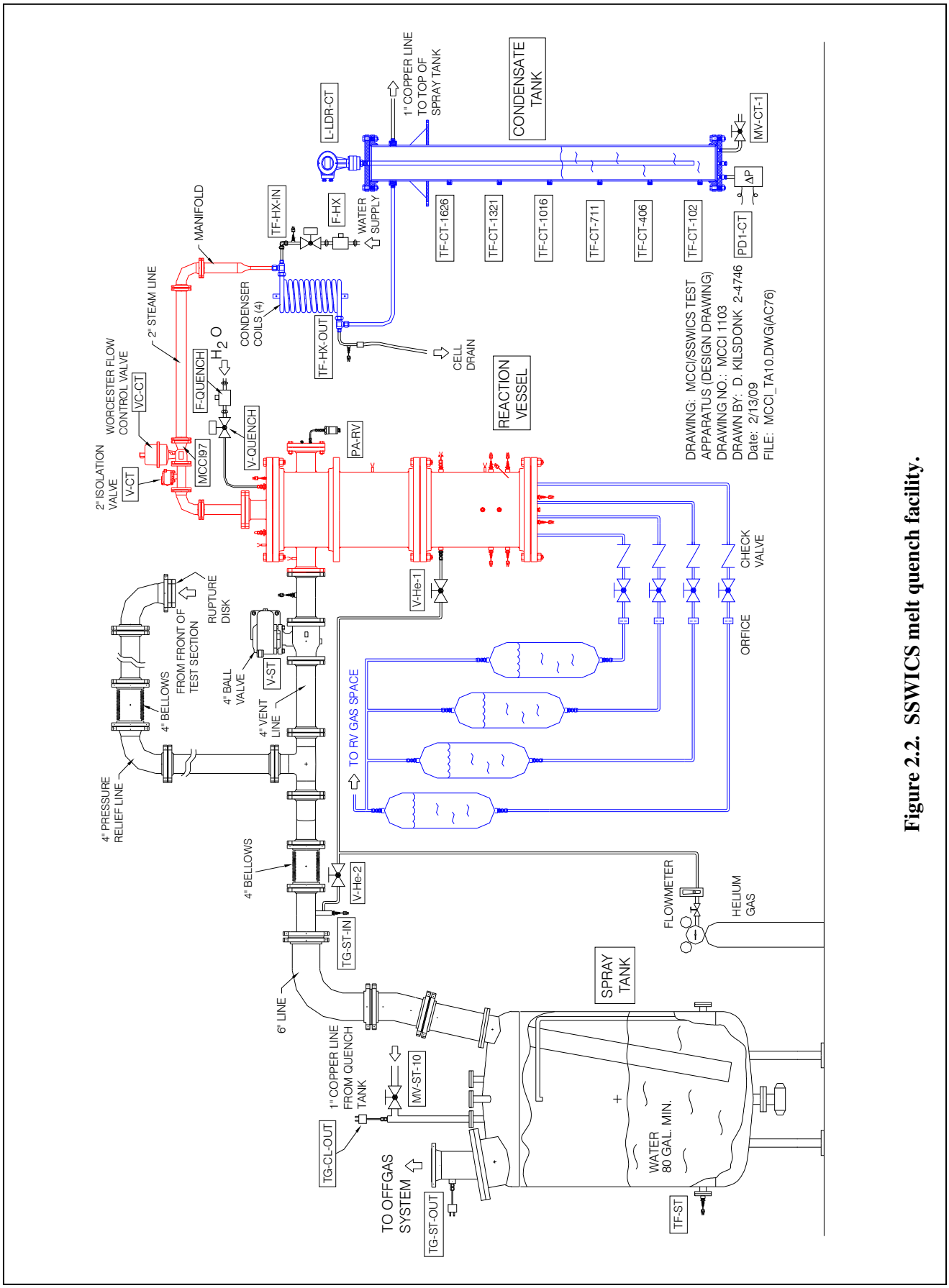

Figure 2.2. SSWICS melt quench facility.

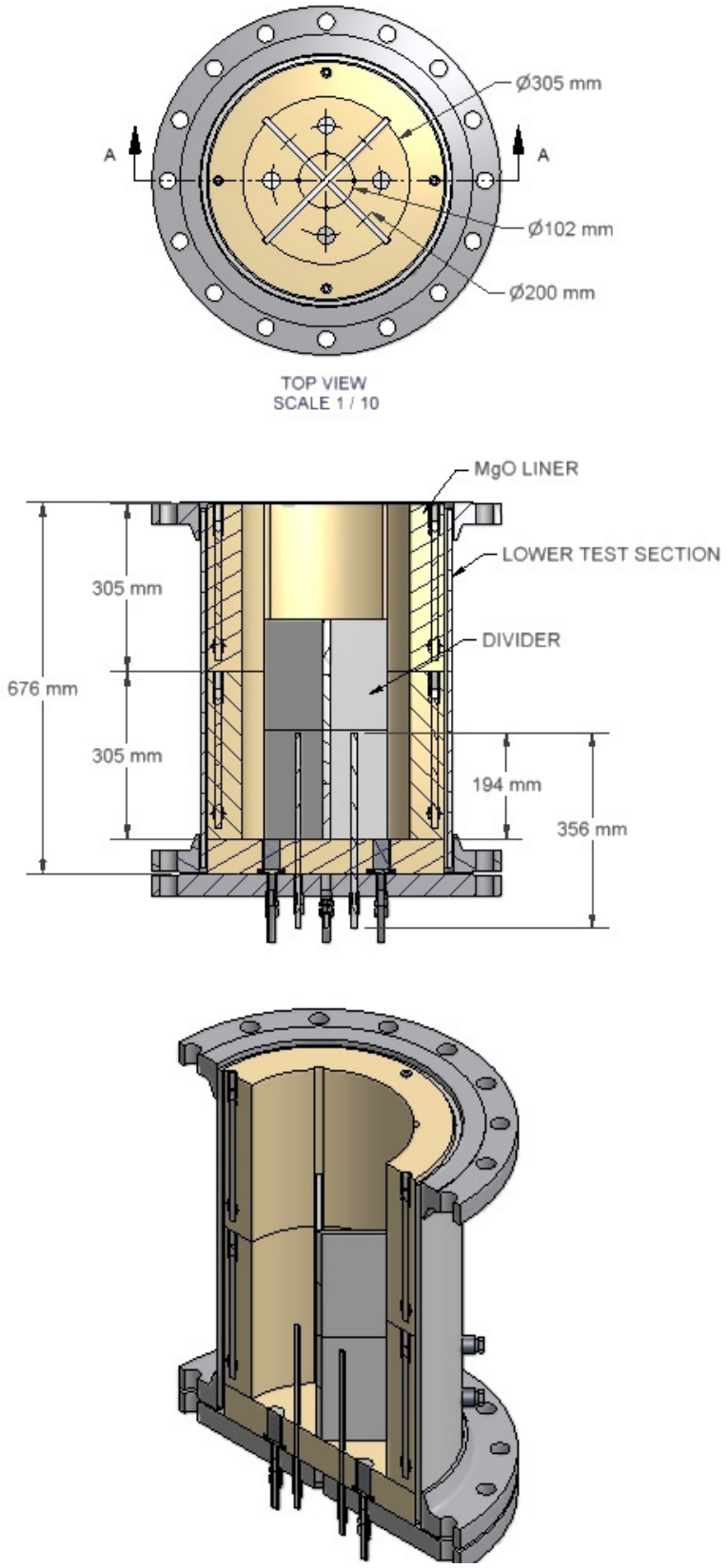

Figure 2.3. Lower plenum and basemat detail.

associated with the corium was calculated to be 0.18 bar by assuming a density of 6000 kg/m^3. Assuming a water head of 10 meters/ bar, the tanks are positioned so that the water surfaces are 2.3, 2.8, 3.3, and 3.8 meters above the bottom of the corium pool.

2.3 Injection Nozzles

The design for the concrete nozzles is shown in Fig. 2.7. Four nozzles are cast within the basemat and positioned so that they are roughly equidistant from the liner and neighboring partitions. The top of each nozzle is flush with the basemat surface and each is filled with porous concrete to provide a path for water flow up into the melt while preventing melt flow downward into the nozzle. The porous concrete filled nozzle is of interest because it mimics a proposed engineered corium cooling system. This separate effect test offers the opportunity to determine the behavior of the nozzle with prototypical corium.

A 0.05 mm-thick stainless steel diaphragm is welded over the top of each nozzle to serve as a temporary seal to prevent water flow from the feed line up into the thermite during the vessel preheat phase of the experiment.

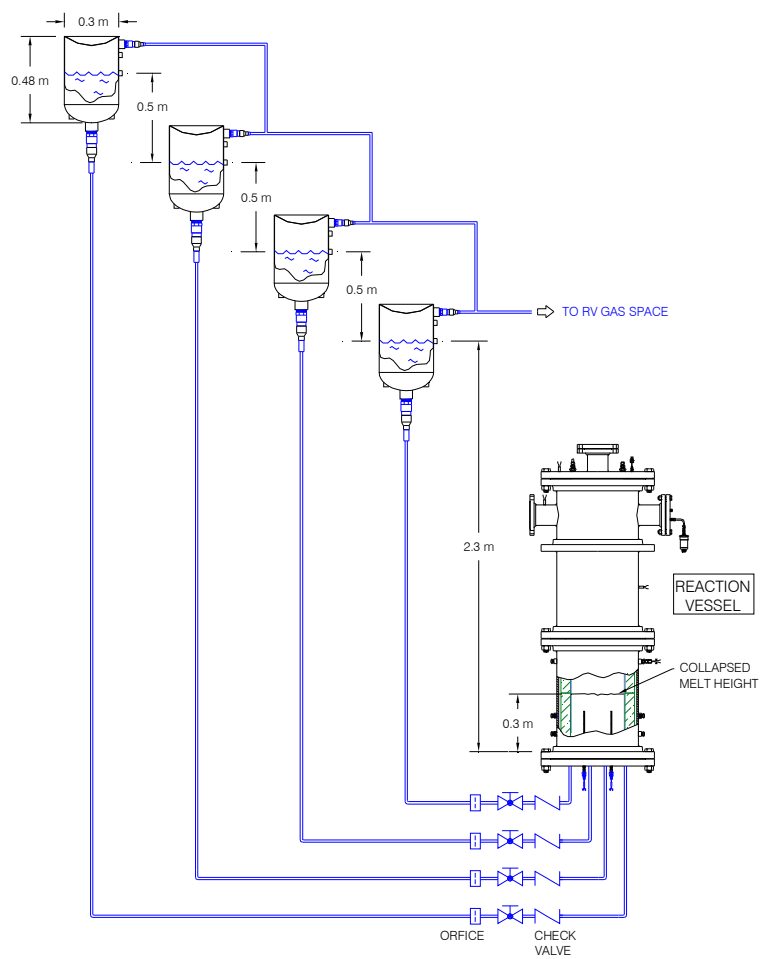

Figure 2.4. Water injection system geometry (drawn to scale).

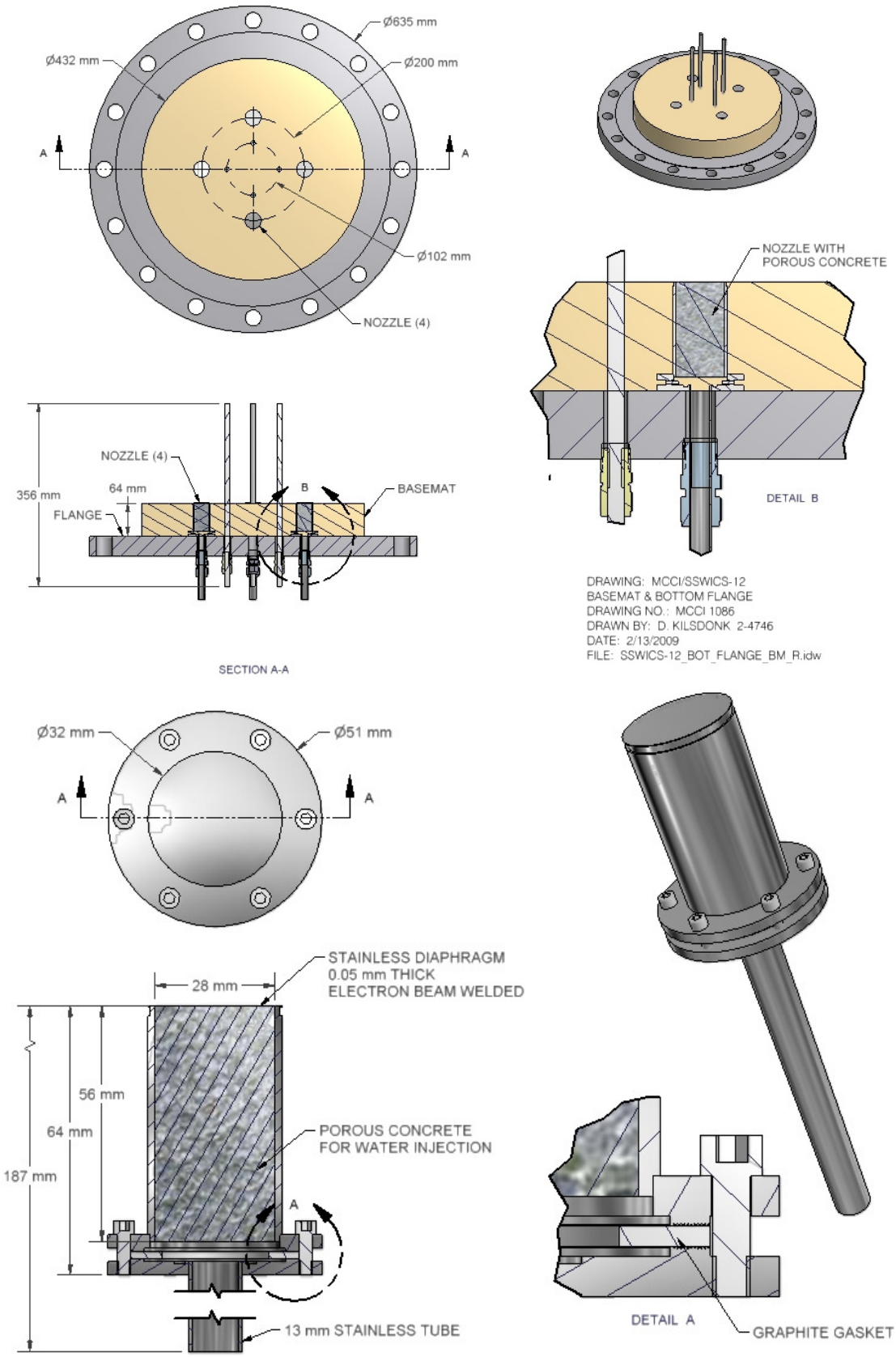

Figure 2.5 Nozzle layout on basemat (top) and nozzle detail (bottom).

3. Data Acquisition and Control Systems

3.1 Instrumentation

This test is intended to determine the efficacy of a particular engineered melt cooling concept. The directive to test a partitioned melt with separate injectors is, in effect, an instruction to combine four quench experiments into one. The instrumentation must therefore provide data sufficient to determine the boundary conditions and cooling behavior of individual partitions. The flow rate and driving pressure of each nozzle is measured along with melt temperatures. The condensate collection and measurement system used in past tests to determine the steaming rate is also used, but it cannot provide the cooling rate of any particular partition. It will instead provide the gross melt cooling rate. Only indirect indications of individual partition cooling rates, obtained through measurements of melt temperature and water flow rate into each quadrant, are available for this test.

Figure 3.1 shows the thermocouple layout in the basemat and the liner. Each partition is allotted a 5-junction C-type thermocouples in tungsten thermowells. The thermocouples are spaced every 51 mm so that the uppermost thermocouple is 190 mm above the basemat surface. The tungsten thermowells are 9.5 mm diameter, which is the same size used in CCI tests but larger than that used in previous SSWICS tests (6 mm). Though thermowell size should be minimized to limit fin cooling effects, the thermowells for this test are too long to fabricate in a diameter less than 9.5 mm.

The nomenclature used to identify thermocouples is as follows: TM (temperature within the corium melt), TF (fluid temperature), TG (gas space temperature), TS (structure temperature), H# (height above the bottom of the melt, in mm, and N, S, E, W representing the cardinal points. The partition is to be situated so that the "wedges" face towards the cardinal points. For example, TM-N-H190 is the melt thermocouple in the north facing wedge, 190 mm above the bottom of the melt. An instrument list is provided in Tables 3.1.

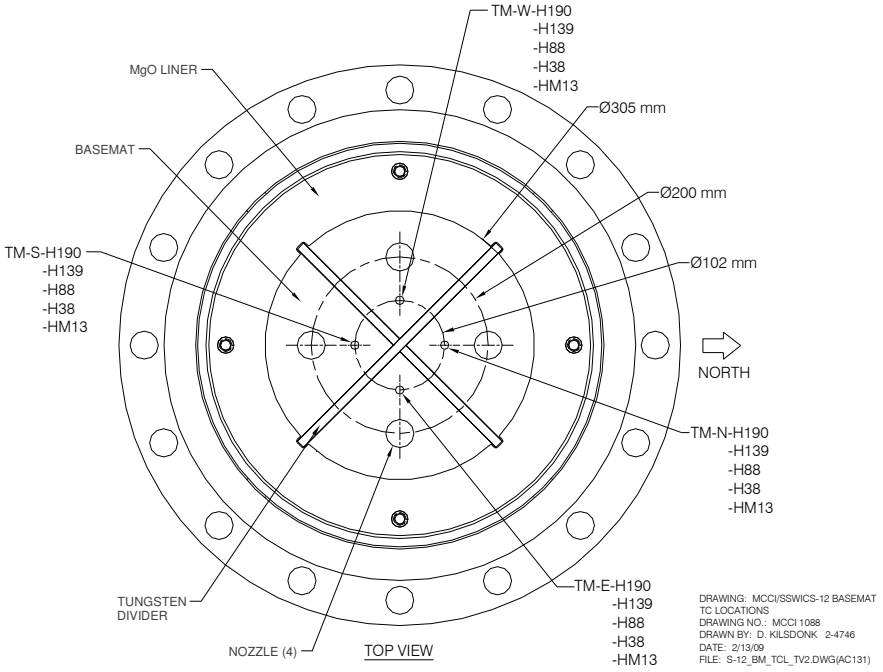

Figure 3.1. Melt thermocouple locations.

#	Channel	Name	Type	Description	Serial #	Output	Range	Accuracy
0	HPS-0	T-CJ-HPS	AD592 IC	Cold junction compensation sensor.	-	1ξA/K	0-70°C	±0.5°C
1	HPS-1	TM-N-H190	TC type C	Melt temp. 190 mm above bottom of melt (in tungsten thermowell).	-	0-37 mV	0-2320°C	±4.5°C or 1%
2	HPS-2	TM-N-H139	TC type C	Melt temp. 139 mm above bottom of melt (in tungsten thermowell).	-	0-37 mV	0-2320°C	±4.5°C or 1%
3	HPS-3	TM-N-H88	TC type C	Melt temp. 88 mm above bottom of melt (in tungsten thermowell).	-	0-37 mV	0-2320°C	±4.5°C or 1%
4	HPS-4	TM-N-H38	TC type C	Melt temp. 38 mm above bottom of melt (in tungsten thermowell).	-	0-37 mV	0-2320°C	±4.5°C or 1%
5	HPS-5	TM-N-Hm13	TC type C	Melt temp. 13 mm below bottom of melt (in tungsten thermowell).	-	0-37 mV	0-2320°C	±4.5°C or 1%
6	HPS-6	TM-S-H190	TC type C	Melt temp. 190 mm above bottom of melt (in tungsten thermowell).	-	0-37 mV	0-2320°C	±4.5°C or 1%
7	HPS-7	TM-S-H139	TC type C	Melt temp. 139 mm above bottom of melt (in tungsten thermowell).	-	0-37 mV	0-2320°C	±4.5°C or 1%
8	HPS-8	TM-S-H88	TC type C	Melt temp. 88 mm above bottom of melt (in tungsten thermowell).	-	0-37 mV	0-2320°C	±4.5°C or 1%
9	HPS-9	TM-S-H38	TC type C	Melt temp. 38 mm above bottom of melt (in tungsten thermowell).	-	0-37 mV	0-2320°C	±4.5°C or 1%
10	HPS-10	TM-S-Hm13	TC type C	Melt temp. 13 mm below bottom of melt (in tungsten thermowell).	-	0-37 mV	0-2320°C	±4.5°C or 1%
11	HPS-11	TM-E-H190	TC type C	Melt temp. 190 mm above bottom of melt (in tungsten thermowell).	-	0-37 mV	0-2320°C	±4.5°C or 1%
12	HPS-12	TM-E-H139	TC type C	Melt temp. 139 mm above bottom of melt (in tungsten thermowell).	-	0-37 mV	0-2320°C	±4.5°C or 1%
13	HPS-13	TM-E-H88	TC type C	Melt temp. 88 mm above bottom of melt (in tungsten thermowell).	-	0-37 mV	0-2320°C	±4.5°C or 1%
14	HPS-14	TM-E-H38	TC type C	Melt temp. 38 mm above bottom of melt (in tungsten thermowell).	-	0-37 mV	0-2320°C	±4.5°C or 1%
15	HPS-15	TM-E-Hm13	TC type C	Melt temp. 13 mm below bottom of melt (in tungsten thermowell).	-	0-37 mV	0-2320°C	±4.5°C or 1%
16	HPS-16	TM-W-H190	TC type C	Melt temp. 190 mm above bottom of melt (in tungsten thermowell).	-	0-37 mV	0-2320°C	±4.5°C or 1%
17	HPS-17	TM-W-H139	TC type C	Melt temp. 139 mm above bottom of melt (in tungsten thermowell).	-	0-37 mV	0-2320°C	±4.5°C or 1%
18	HPS-18	TM-W-H88	TC type C	Melt temp. 88 mm above bottom of melt (in tungsten thermowell).	-	0-37 mV	0-2320°C	±4.5°C or 1%
19	HPS-19	TM-W-H38	TC type C	Melt temp. 38 mm above bottom of melt (in tungsten thermowell).	-	0-50 mV	0-1250°C	±2.2°C or 0.75%
20	HPS-20	TM-W-Hm13	TC type C	Melt temp. 13 mm below bottom of melt (in tungsten thermowell).	-	0-50 mV	0-1250°C	±2.2°C or 0.75%
21	HPS-21	TG-RV	TC type C	Gas temp. in reaction vessel upper plenum.	-	0-50 mV	0-1250°C	±2.2°C or 0.75%
22	HPS-22	TS-RV-tf	TC type K	Temperature of RV top flange.	-	0-50 mV	0-1250°C	±2.2°C or 0.75%
23	HPS-23	TS-RV-1000	TC type K	Outer wall temp. of RV 1000 mm above bottom of melt.	-	0-50 mV	0-1250°C	±2.2°C or 0.75%
24	HPS-24	TS-RV-mf	TC type K	Temperature of RV middle flange.	-	0-50 mV	0-1250°C	±2.2°C or 0.75%
25	HPS-25	TS-RV-100	TC type K	Outer wall temp. of RV 100 mm above bottom of melt.	-	0-50 mV	0-1250°C	±2.2°C or 0.75%
26	HPS-26	TS-RV-bf	TC type K	Temperature of RV bottom flange.	-	0-50 mV	0-1250°C	±2.2°C or 0.75%
27	HPS-27	TS-vent	TC type E	Outer wall temp. of vent line.	-	0-70 mV	0-900°C	±1.7°C or 0.5%
28	HPS-28	TF-CT-102	TC type K	Fluid temp. in condensate tank at a water level of 102 mm.	-	0-50 mV	0-1250°C	±2.2°C or 0.75%
29	HPS-29	TF-CT-406	TC type K	Fluid temp. in condensate tank at a water level of 406 mm.	-	0-50 mV	0-1250°C	±2.2°C or 0.75%
30	HPS-30	TF-CT-711	TC type K	Fluid temp. in condensate tank at a water level of 711 mm.	-	0-50 mV	0-1250°C	±2.2°C or 0.75%
31	HPS-31	TF-CT-1016	TC type K	Fluid temp. in condensate tank at a water level of 1016 mm.	-	0-50 mV	0-1250°C	±2.2°C or 0.75%
32	HPS-32	TF-CT-1321	TC type K	Fluid temp. in condensate tank at a water level of 1321 mm.	-	0-50 mV	0-1250°C	±2.2°C or 0.75%
33	HPS-33	TF-CT-1626	TC type K	Fluid temp. in condensate tank at a water level of 1626 mm.	-	0-50 mV	0-1250°C	±2.2°C or 0.75%
34	HPS-34	TF-HX-in	TC type K	Fluid temp. at HX coolant inlet.	-	0-50 mV	0-1250°C	±2.2°C or 0.75%
35	HPS-35	TF-HX-out	TC type K	Fluid temp. at HX coolant outlet.	-	0-50 mV	0-1250°C	±2.2°C or 0.75%

Table 3.1. Instrumentation list for water ingression tests (part 1 of 2).

36	HPS-36	HF-vent	Thermopile	Heat Flux through connecting line to V-ST.	0632	0-5.50 mV	0-5 kW/m^2	±3%
37	HPS-37	I-ign	DC supply	Current supply for thermite ignitor.	-	0-100 mV	0-25 Amps	-
38	HPS-38	TF-quench	TC type K	Temperature of water injected into RV	-	0-50 mV	0-1250°C	±2.2^{o}C or 0.75%
39	HPS-39	Reserve	-	-	-	-	-	-
40	HPS-40	PA-RV	1810AZ	Absolute pressure in reaction vessel.	02351-00P1PM	1-6 V	0-14 bar gage	±0.14 bar
41	HPS-41	PD-CT	1801DZ	ξP transmitter to measure condensate inventory.	-	0-13 V	0-0.35 bar	±0.004 bar
42	HPS-42	L-TDR-CT	BM100A	Time domain reflectometer to measure CT level.	A02331879A	4 - 20 mA	0 - 2 m	±3 mm
43	HPS-43	VDC-P-supply	-	Voltage of the power supply for the pressure transmitters.	-	0 - 15 V	-	-
44	HPS-44	Reserve	-	-	-	0 - 5 V	0-50 sl/m Ar	±0.5 sl/m
45	HPS-45	Reserve	-	-	-	0-37 mV	0-2320°C	±4.5^{o}C or 1%
46	HPS-46	Reserve	-	-	-	0-37 mV	0-2320°C	±4.5^{o}C or 1%
47	HPS-47	Reserve	-	-	-	0-37 mV	0-2320°C	±4.5^{o}C or 1%
48	HPS-48	Reserve	-	-	-	0-37 mV	0-2320°C	±4.5^{o}C or 1%
49	HPS-49	Reserve	-	-	-	0-37 mV	0-2320°C	±4.5^{o}C or 1%
50	HPS-50	Reserve	-	-	-	0-37 mV	0-2320°C	±4.5^{o}C or 1%
51	HPS-51	PD-R05	-	ξP transmitter to measure level in reservoir with 0.5 m head.	-	0-13 V	0-0.35 bar	±0.004 bar
52	HPS-52	PD-R1	-	ξP transmitter to measure level in reservoir with 1.0 m head.	-	0-13 V	0-0.35 bar	±0.004 bar
53	HPS-53	PD-R15	-	ξP transmitter to measure level in reservoir with 1.5 m head.	-	0-13 V	0-0.35 bar	±0.004 bar
54	HPS-54	PD-R2	-	ξP transmitter to measure level in reservoir with 2.0 m head.	-	0-13 V	0-0.35 bar	±0.004 bar
55	HPS-55	Reserve	-	-	-	-	-	-
56	HPS-56	Reserve	-	-	-	-	-	-
57	HPS-57	Reserve	-	-	-	-	-	-
58	HPS-58	Reserve	-	-	-	-	-	-
59	HPS-59	Reserve	-	-	-	-	-	-
60	HPQ-50	T-CJ-HPQ	AD592 IC	Cold junction compensation sensor.	-	1ξA/K	0-70°C	±0.5^{o}C
61	HPQ-51	TF-ST	TC type K	Fluid temp. in spray tank.	-	0-50 mV	0-1250°C	±2.2^{o}C or 0.75%
62	HPQ-52	TG-CL-out	TC type K	Gas temperature in condensate tank outlet line to spray tank.	-	0-50 mV	0-1250°C	±2.2^{o}C or 0.75%
63	HPQ-53	TG-ST-in	TC type K	Gas temp. in the spray tank line inlet.	-	0-50 mV	0-1250°C	±2.2^{o}C or 0.75%
64	HPQ-54	TG-ST-out	TC type K	Gas temp. in the spray tank line outlet.	-	0-50 mV	0-1250°C	±2.2^{o}C or 0.75%
65	HPQ-55	F-quench	Paddlewheel	Flow rate of water into reaction vessel (for quenching melt).	3144	0-5 V	0-50 gpm	±0.5 gpm
66	HPQ-56	F-HX	Paddlewheel	Flow rate of cold water to heat exchangers.	3143	0-5 V	0-50 gpm	±0.5 gpm

Table 3.1. (continued).

LabVIEW Channel #	Valve Name	Description	Actuator
1	V-CT	Valve on steam line between reaction vessel and quench tank.	Pneumatic
2	V-quench	Valve on quench water supply line into reaction vessel.	Solenoid
3	V-quench-i	Isolation valve on quench water supply line into reaction vessel.	Solenoid
4	V-quench-b	Valve on back-up quench water supply.	Solenoid
5	V-ST	Valve on vent line between reaction vessel and spray tank.	Pneumatic
Panel	V-HX	Valve on cooling-water line to heat exchangers.	Solenoid
Panel	VC-CT	Control valve on steam line between reaction vessel and quench tank.	Electric

Table 3.2. Remotely operated valves.

3.2 General

All data acquisition and process control tasks are managed by a PC executing LabVIEW 8.2 under Windows XP. Sensor output terminals are connected to model HP E1345A 16-channel multiplexers and the signals are digitized by an HP E1326B 5 ½ digit multimeter located within the test cell (Fig. 3.2). Signal noise is reduced by integration over a single power line cycle (16.7 ms). The digitized sensor readings are routed from the test cell to the PC in the control room via two HP-IB extenders. The extenders allow the ASCII data from the HP to be sent through the cell wall over a BNC cable. The extender within the control room then communicates with a GPIB card within the PC. This configuration also permits remote control of the multimeter through LabVIEW. The power line cycle integration results in a minimum (theoretical) time of 0.75 s to scan the channel list (16.7 ms * 45 channels). In practice, however, the acquisition of a single scan is at a frequency of approximately 0.5 Hz.

Valves are controlled with the PC using a relay card housed within an SCXI chassis (National Instruments). These electromechanical relays are capable of switching up to 8 A at 125 VAC or 5 A at 30 VDC. They are operated via a switch controller in the SCXI chassis, which communicates with the PC through a general-purpose data acquisition card. As shown in Fig. 3.2, the relays in the control room operate devices within the test cell indirectly, through a second relay. This is intended to provide an additional level of electrical isolation between the NI switching hardware and high voltage sources within the cell. As an added safety measure, all wiring is routed through a control panel that can be switched from automatic (PC) control to manual control in the event of computer failure.

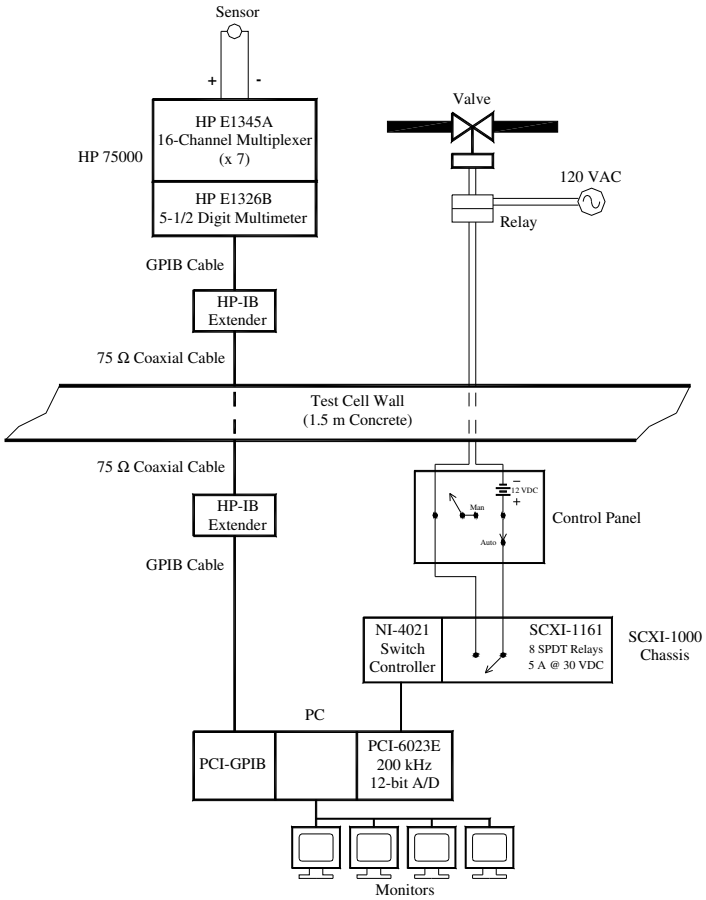

Figure 3.2. Data acquisition and control systems.

4. Test Parameters and Course of Test

The oxide phase of the corium composition for SSWICS-12 is the same as that of SSWICS-6 (60.3/24.7/15.0 wt % UO_2/ZrO_2/siliceous concrete). The thermite was, however, slightly reformulated to react at a higher temperature to minimize crust formation on the basemat that might impair initial water flow through the nozzles. The initial melt temperature for SSWICS-6 was ~1950˚C while the target initial temperature for this test is ~2100˚C. The thermite composition for this test is shown in Tables 4.1. Reformulation of the thermite to produce the higher reaction temperature results in a slightly higher Cr metal byproduct content of 7.6 wt % in the melt, which can be compared to the level of 6.4 wt % for the SSWICS-6 thermite. Test specifications for completed tests are summarized in Table 4.2.

The day before the test, the water injection line orifices (in actuality, needle valves) were adjusted so that each tank would provide an initial flow rate of 0.5 l/min. The adjustments were made over several fill and drain runs. The day of the test, the tanks were each filled with water to a level of ~0.4 m to provide the initial net driving heads of 0.05, 0.1, 0.15, and 0.2 bar. The isolation valves were opened shortly before the cell was closed for ignition of the thermite.

The igniter coil was energized to initiate thermite ignition, which was first detected by a sudden rise in the upper plenum gas temperature TG-RV. Thermocouples within each melt partition began rising 30-60 sixty seconds later.

Within the first minute following ignition the video monitors showed evidence of a small fire around the top RV flange. We took no action for the next two minutes in the hopes that water injection and steam generation would begin cooling the melt and extinguish the fire. We were not able to confirm early water injection through reservoir level changes because of system pressure fluctuations produced by the thermite ignition (and possibly the water injection itself).

Sporadic signs of fire continued and at t=120 s there was still no clear evidence of water injection from the reservoirs. It is now known that water injection had indeed occurred and the resulting steam generation had ejected melt upward to coat the entire inner surface of the RV, including the lid.

At t=140 s water injection from above was initiated by opening the isolation valve on the back-up

Constituent	Mass (kg)
U_3O_8	78.61
CrO_3	19.90
CaO	2.96
Zr	22.98
Mg	0.10
Si	3.51
SiO_2	7.49
Al	0.45
Total	136.0

Constituent	Wt %	
	Reactant	Product
U_3O_8	57.80	-
UO_2	-	55.61
Zr	16.90	-
ZrO_2	-	22.84
Si	2.58	-
SiO_2	5.51	11.03
Mg	0.07	-
MgO	-	0.11
Al	0.33	-
Al_2O_3	-	0.63
CaO	2.18	2.18
CrO_3	14.63	-
Cr	-	7.60

Tables 4.1. Corium powder charge and reaction product mass fractions.

Table 4.2 Test specifications for completed SSWICS experiments.

Parameter	Test Number											
	1	**2**	**3**	**4**	**5**	**6**	**7**	**8**	**9**	**10**	**11**	**12**
Melt composition (wt% UO_2/ZrO_2/Cr/ Concrete)	61/25/6/8	61/25/6/8	61/25/6/8	48/20/9/23	56/23/7/14	56/23/6/14	64/26/6/4	56/23/6/14	56/23/6/14	61/25/6/8	56/23/6/14	56/23/6/14
Concrete type	LCS	SIL	LCS	LCS	LCS	SIL	LCS	SIL	SIL	SIL	SIL	SIL
Melt mass (kg)	75	75	75	60	68	68	80	68	23	25	68	136
Melt depth (cm)	15	15	15	15	15	15	15	15	5	5	15	30
Initial Melt Temperature (^oC)	~2300	~2100	~2100	~2100	~2100	~1950	~2100	~1900	-	-	~1850	~2000
System pressure (bar)	1	1	4	4	4	1	4	1	1	1	1	1
Water injection flowrate (lpm)	4	4	12	13	6	14	13	10	9	9	-	-
Water injected (liters)	33	39	34	40	61	47	40	41	20	29	>30	~100
Test date (day/mo/year)	30/08/02	17/09/02	30/01/03	13/03/03	15/10/03	24/02/04	14/12/04	25/01/07	14/02/08	5/03/08	11/05/08	09/04/09

supply line (V-quench in Fig. A.6). The line was open for approximately 9 minutes. A temperature increase on the heat exchanger outlet appeared at 150 s and the condensate tank water level began to rise at 190 s. Note that the valve to the surge tank was open until ~220 s and so it is likely that, until then, most of the steam flowed to the surge tank rather than the condenser. Figure A.6 shows an initial ramp up in pressure that begins with thermite ignition and then a drop at 170 s, about 30 s after top flooding was started. The pressure drop continued until the surge tank valve was closed. It then quickly rose to the test peak of 1.9 bar

Each partition reached a peak temperature of ~2000°C within 200 seconds. Figures A.1-A.4 show the melt temperatures measured during the transient (all plots are attached as an appendix). All data has been plotted so that the x-axis origin corresponds with the initial rise in TG-RV. Melt temperatures began to rapidly decline after water injection and all melt thermocouples reached the saturation temperature by 4400 s, when the test was terminated.

5. Sensor Malfunctions and Abnormalities

Post test examination of the test apparatus and a preliminary review of the data indicate the following:

1) Bottom injection through the porous nozzles was supplemented by injection from above out of concern for the integrity of the RV. There is no flow meter on this emergency line and it is estimated that ~40 liters were injected from above.
2) The measurements of reservoir level are considered to be in error. The configuration used employs gauge ΔP measurements where one transducer port is on the tank and the other at ambient pressure. The transducers are designed for dry gas only on the high port and so direct ΔP measurements across the water-filled tank were not possible. Because the system pressure is not held at ambient, level must be calculated using both the gauge measurement and the absolute pressure in the reservoirs, which is assumed to be the pressure measured for the RV. A pressure equalization line connects the reservoirs to the RV. Level calculations have produced unreasonable results and it is thought likely that the equalization line was blocked by corium. A graph of measured reservoir versus ΔP has been included nevertheless because it indicates that the tanks all emptied at about the same rate, as planned (Fig. A.13).

6. Data Reduction

Some simple calculations have been performed to provide a preliminary assessment of the test data. The first is a calculation of the coolant inventory in the RV as a function of time. The inventory is the difference between the total amount of liquid injected and the amount boiled off and collected in the CT:

$$M_{H_2O-RV} = \sum_{t=0}^{t=t_{end}} \rho \dot{V} \Delta t \quad - \quad \frac{\pi}{4} D^2 \frac{\Delta P}{g} \tag{6.1}$$

where data from sensor F-quench is used for the volumetric flow rate $\dot{V}$ and the liquid density ρ is taken to be 998 kg/m^3. The condensate inventory is calculated with readings from sensor PD-CT (ΔP) and the tank diameter D of 0.203 m.

The corium heat flux was calculated using two different methods. The first considers the rate of condensate collection, which is a measure of the steam flow rate from the RV. Accurate determination of

the heat flux at the corium surface must, however, account for various heat sinks. During the injection phase, energy is absorbed raising the coolant to the saturation temperature. Some of the vapor produced by the quenching melt condenses on the walls of the upper plenum to heat the RV structures to the saturation temperature. Later, heat losses from the upper plenum generate continued condensation. Accounting for these heat sinks, the rate of energy transfer through the corium surface is written as:

$$Q = M_{RV}\, c_p \frac{\partial T}{\partial t} + \dot{m}\, h_{fg} + [M_S c_M \frac{\partial T}{\partial t} + Q_{HL}]\Big|_{up} \tag{6.2}$$

where $\dot{m}$ is mass flow rate of condensate into the CT, M_S is the mass of the RV upper plenum structures, c_M is their heat capacity,, and Q_{HL} represents total upper plenum heat losses. For this report, liquid subcooling has been neglected (an accurate assumption after the injection phase) along with heat losses and time variations in structure temperatures. The condensation rate is calculated from the time derivative of the differential pressure signal PD-CT. The heat transfer rate from the corium is then:

$$Q = \frac{1}{g}\frac{\pi}{4} D^2 \frac{\partial \Delta P}{\partial t} h_{fg} \tag{6.3}$$

where D is again the inner diameter of the CT and the heat of vaporization h_{fg} is 2256 kJ/kg^{o}C (TG-RV registered 100°C through most of the transient). The heat flux is obtained by scaling Q with the initial surface area of the corium (0.071 m^2). The derivative was calculated with pairs of averaged ΔP readings (an average of 5 measurements at 0.5 Hz) centered around a Δt of 60 s. The averaging and length of Δt were necessary to reduce oscillations in the calculated heat flux.

The second method of calculating corium heat flux uses an energy balance on the secondary side of the heat exchanger. The measured parameters are the coolant flow rate on the secondary side of the cooling coils and the inlet and outlet coolant temperatures. The cooling power of the heat exchanger is then:

$$Q_{HX} = \rho \dot{V}_{HX}\, c_p (T_{out} - T_{in}) \tag{6.4}$$

where readings from sensors TF-HX-in and TF-HX-out were used for temperatures T_{in}, and T_{out}, respectively. Data from the flow meter F-HX was used for $\dot{V}_{HX}$ while the density and heat capacity of water were taken to be 982 kg/m^3 and 4.18 kJ/kg^{o}C, respectively.

The cooling power of the heat exchanger is related to the steam flow rate out of the RV by the following:

$$Q_{HX} = \dot{m}\,[h_{fg} + c_p (T_{sat} - T_{con})] \tag{6.5}$$

where $\dot{m}$ is the mass flow rate of steam into the heat exchanger (identical to the flow rate of condensate into the CT, as defined in equation 5.2). From equation 6.5 it can be seen that if condensate leaves the heat exchanger at the saturation temperature, i.e., there is no subcooling, the cooling power of the heat exchanger is equal to the product of $\dot{m}$ and h_{fg}. In this case, according to equation 6.2, the cooling power of the heat exchanger equals the heat transfer rate from the melt. However, the condensate does not, in general, leave the heat exchanger at the saturation temperature. The result of this subcooling is an overestimation of the corium heat flux when using equation 6.5 and the assumption of $T_{sat} = T_{con}$.

The corium heat flux could be calculated more accurately with the heat exchanger energy balance through the addition of a condensate temperature measurement at the heat exchanger outlet. However, the calculation would still require the steam mass flow rate, which would be derived from the CT level measurements. Thus the heat exchanger energy balance, with the assumption of $T_{sat} = T_{con}$, is considered

to be a rough check of the heat flux measurements derived directly from the CT level measurements using equation 6.3.

7. Post Test Exams

This was the first SSWICS test with bottom water injection and it is the only test in which melt was ejected up above the MgO liners. We have included photos taken during disassembly to show the corium distribution. Figure 7.1 shows the lower assembly with all three MgO liners in place (the top liner is identified from its green color as it was used in the previous test). Figure 7.2 shows the lower assembly after the test. Only two of the liners are present in this photo. The corium coating the liner walls and tungsten plates is approximately 2 cm thick. Figure 7.3 shows a wide view of the assembly that includes the pressure vessel.

Figure 7.4 shows the inside of the upper plenum. The view is looking up into the pressure vessel after the lower assembly was removed. The circular plate seen in the center of the photo is the baffle used to prevent water droplets from flowing directly up into the steam line (Fig. 2.1). The ¼" stainless steel tubes used for the four water injection lines are completely melted away. The steel liner above the third MgO liner is completely coated with corium and most of the baffle is also coated.

Figures 7.5 and 7.6 show the basemat before and after the test. Close examination of Fig. 7.6 confirms that each nozzle diaphragm melted as planned and that the porous concrete remained within the nozzle housing.

Figure 7.7 shows the distribution of corium collected from the vessel. As the apparatus was disassembled, corium was scraped from selected zones, collected and weighed. The top zone includes the underside of the flange and baffle and the sides of the pressure vessel above the steel liner. The second zone consists of the steel liner and the third corresponds to the top MgO liner. The fourth zone extends from the top of the second liner down to the top of the tungsten partition and corium in the remainder of the vessel is grouped into the fifth zone. Note that corium occasionally fell from the walls during disassembly. Also, corium from one zone might fall off during collection of corium from a neighboring zone and so there was some mixing of material from various zones. The uncertainty in the mass values given in Fig. 7.7 is estimated to be +/-20%. It is likely, however, that the uncertainty is not random and that the masses for the upper regions are skewed slightly low while those of the lower plenum are high (as some corium fell into the lower plenum during disassembly).

Figure 7.1. Top view of lower plenum pretest.

Figure 7.2 Top view of lower plenum post test

Figure 7.3. Lower plenum showing crust above tungsten partition.

Figure 7.4 View of top flange looking upward through upper plenum.

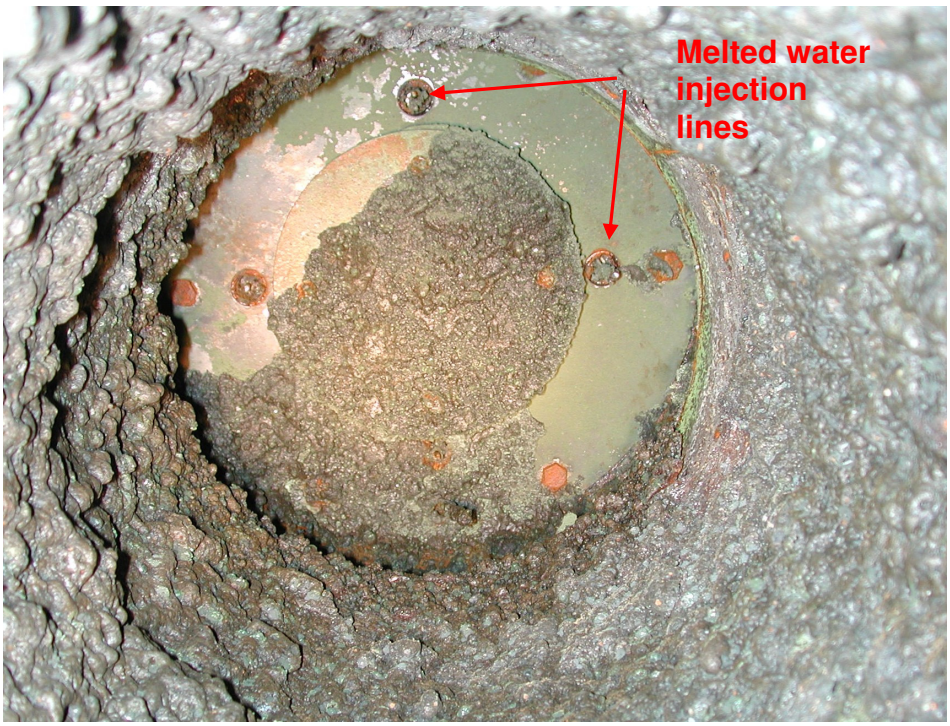

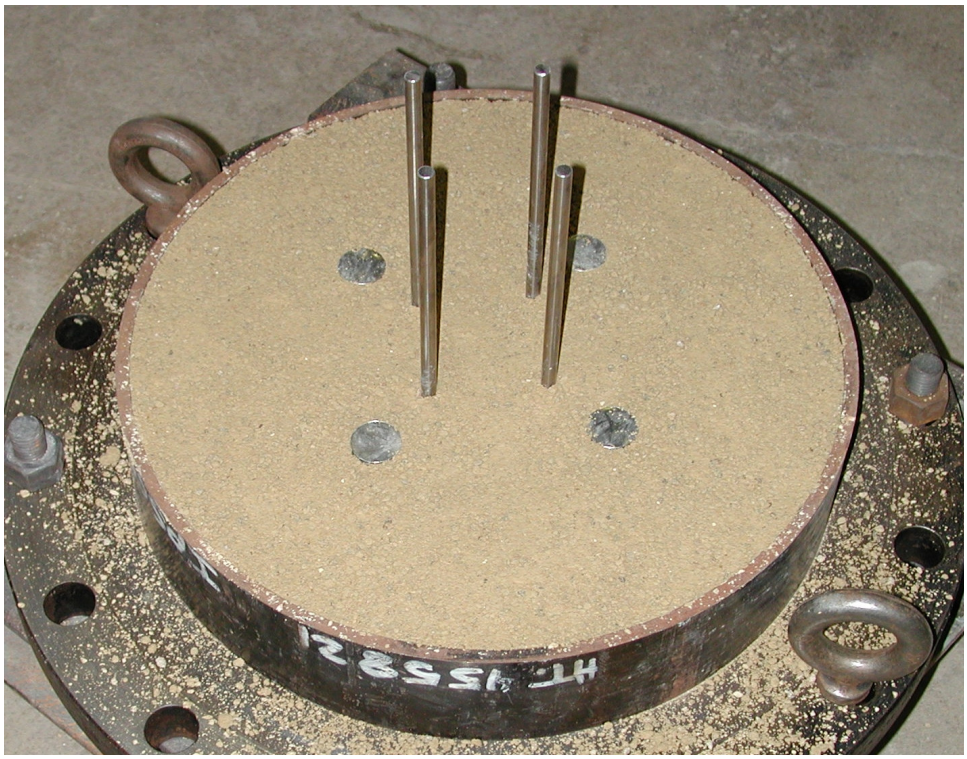

Figure 7.5. Basemat assembly pretest.

Figure 7.6 Basemat assembly posttest.

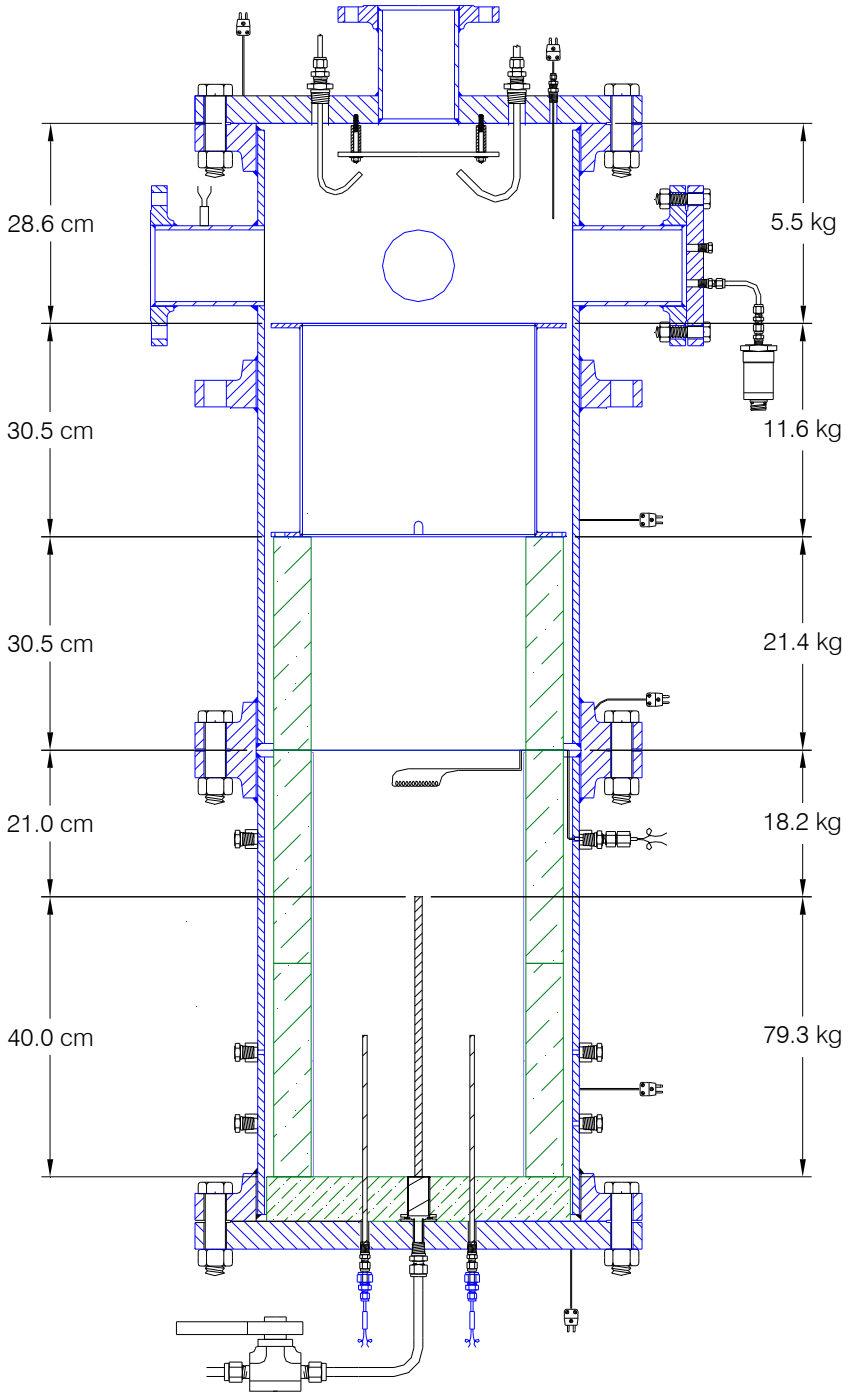

Figure 7.7. Posttest corium distribution. Crust was collected from each of the top four regions shown and then weighed. The mass for the lowest elevation is assumed to be the balance from the initial 136 kg thermite charge.

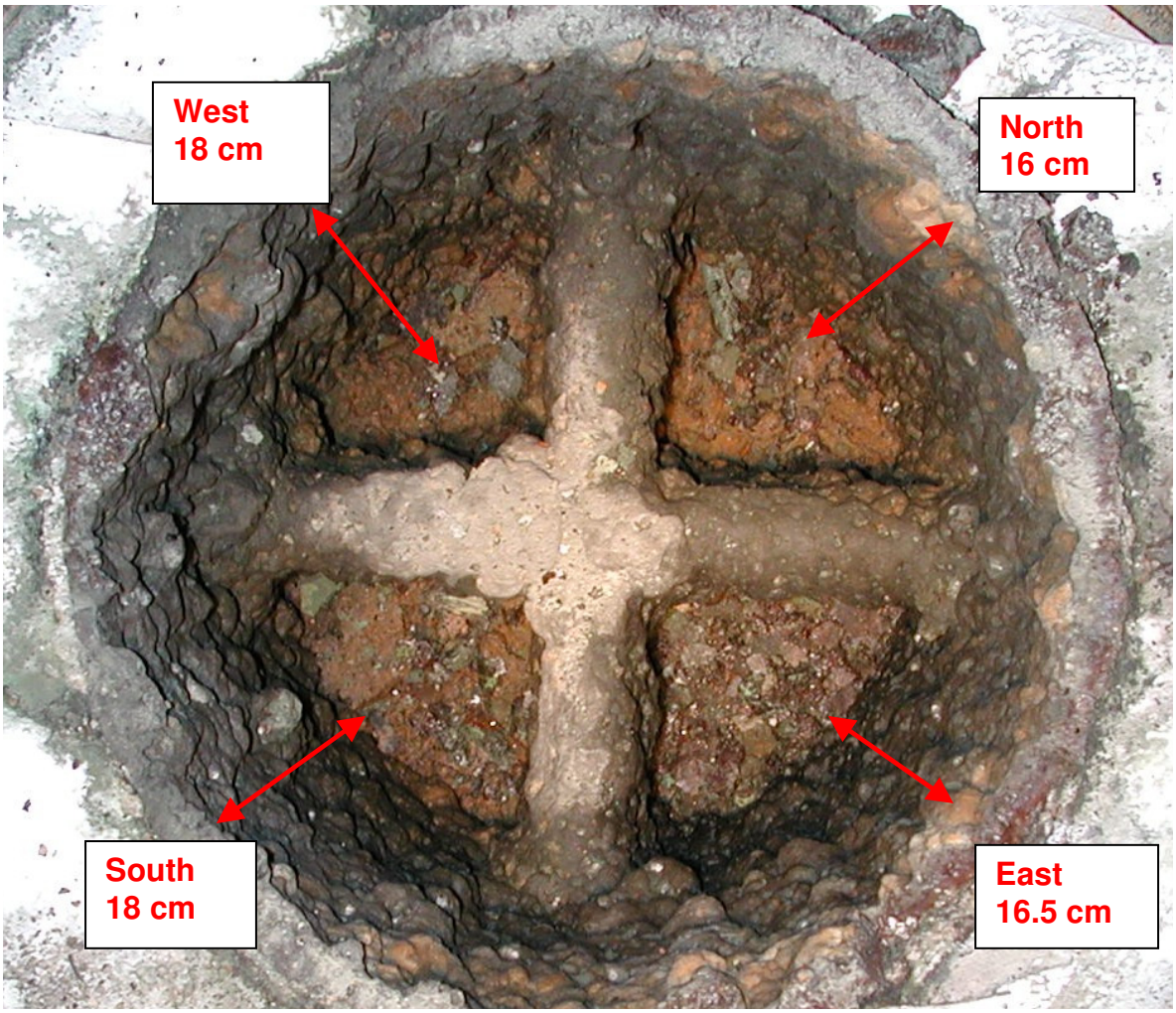

Figure 7.8. Corium levels in each partition. The level was measured from corium to top of MgO liner, which is 60 cm above the basemat. Corium depths are therefore: north 44 cm, east 43.5 cm, south and west 42 cm.

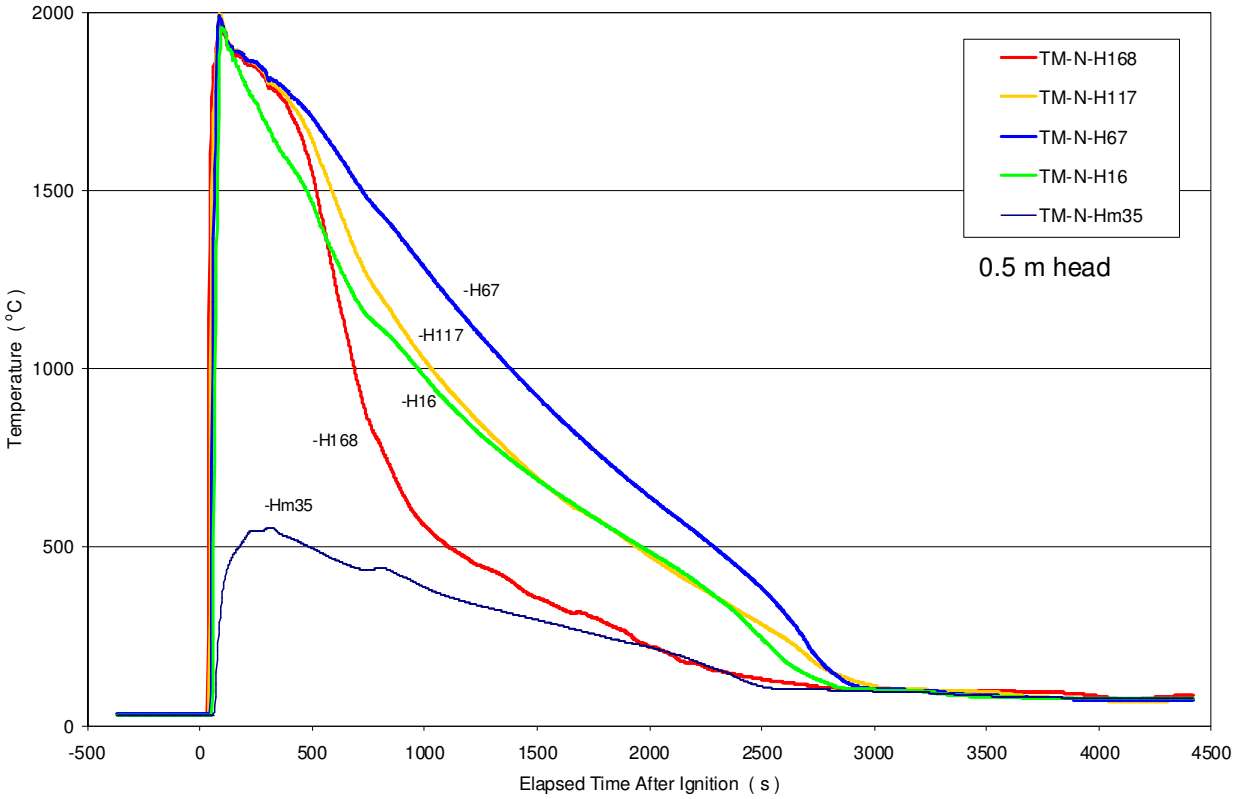

Figure A.1 Temperatures in tungsten thermowell; north melt quadrant.
Figure A.2 Temperatures in tungsten thermowell; south melt quadrant.

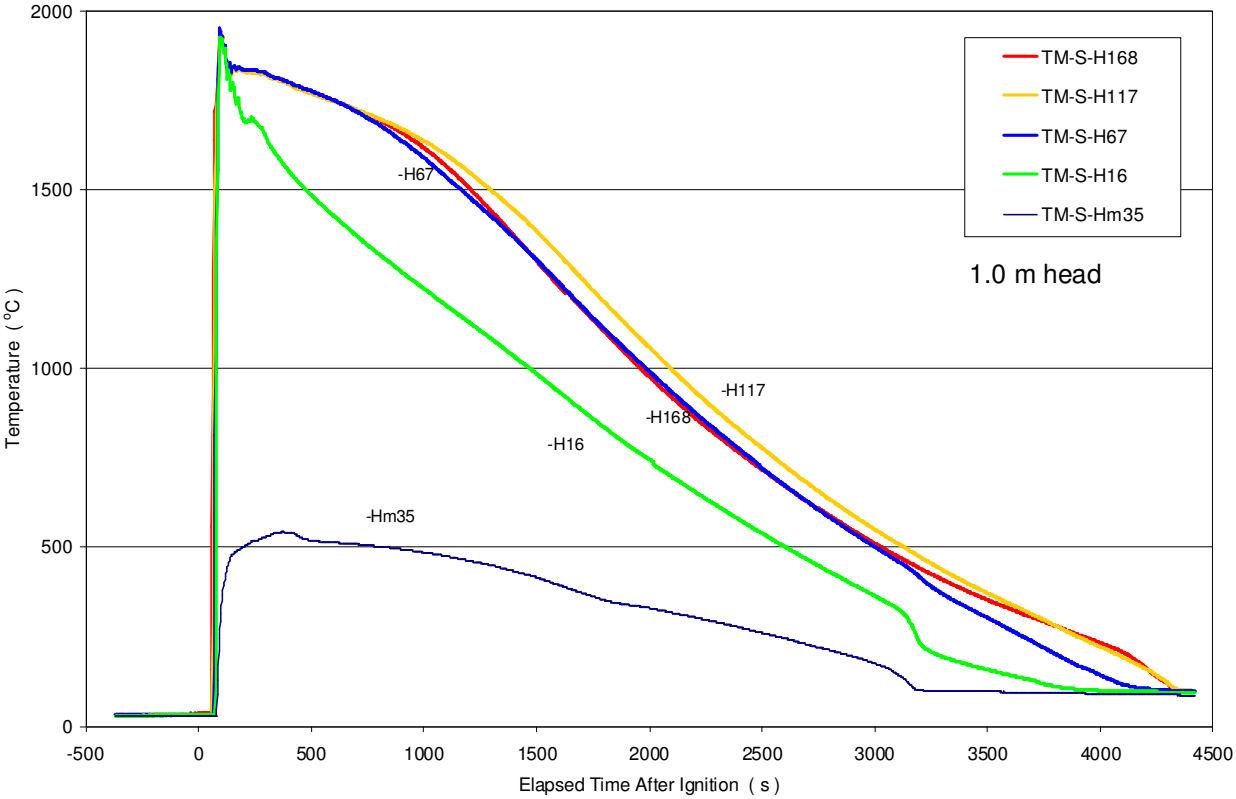

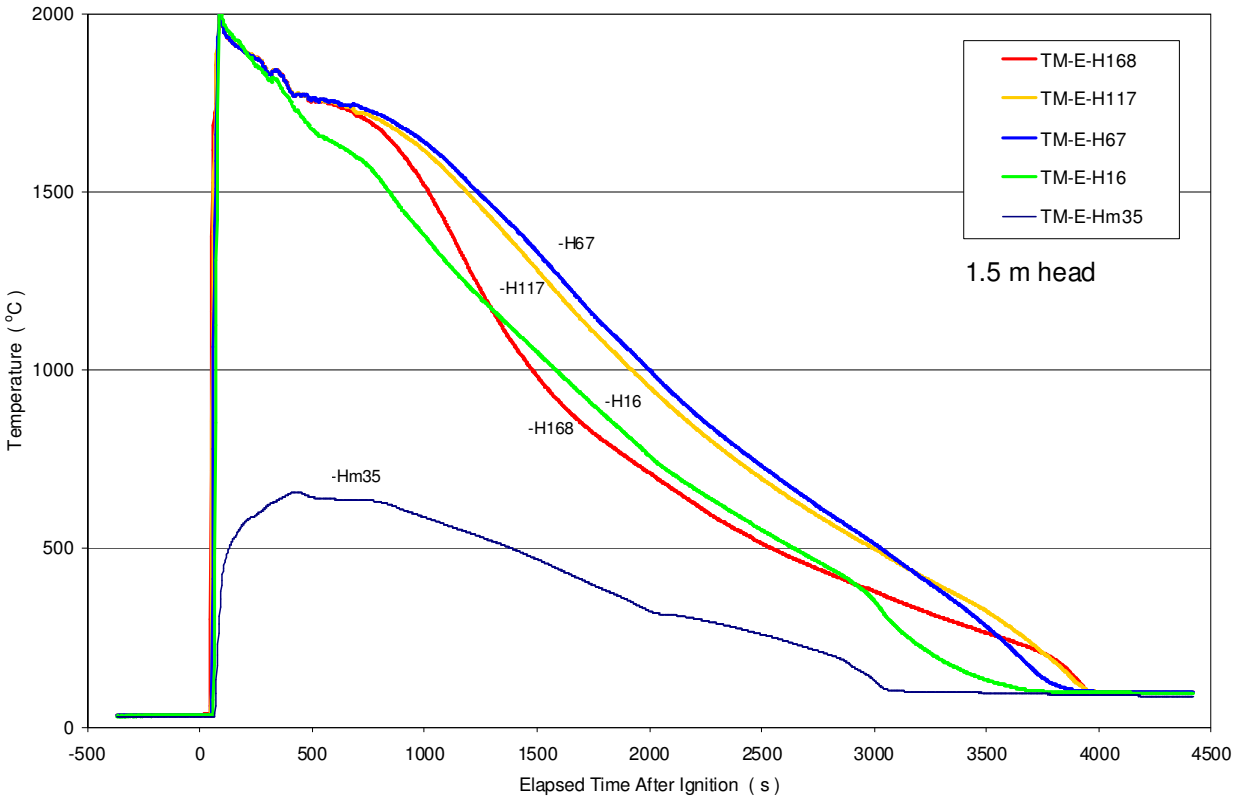

Figure A.3 Temperatures in tungsten thermowell; east melt quadrant.
Figure A.4 Temperatures in tungsten thermowell; west melt quadrant.

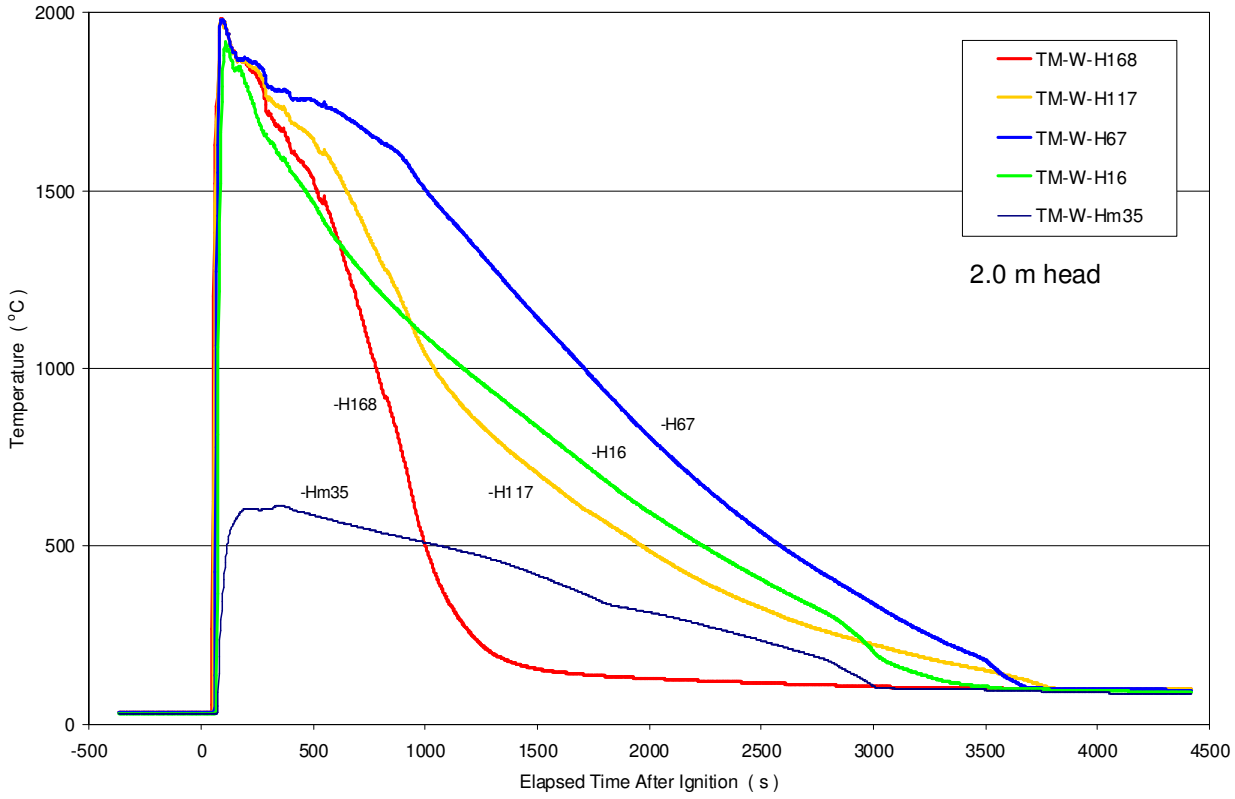

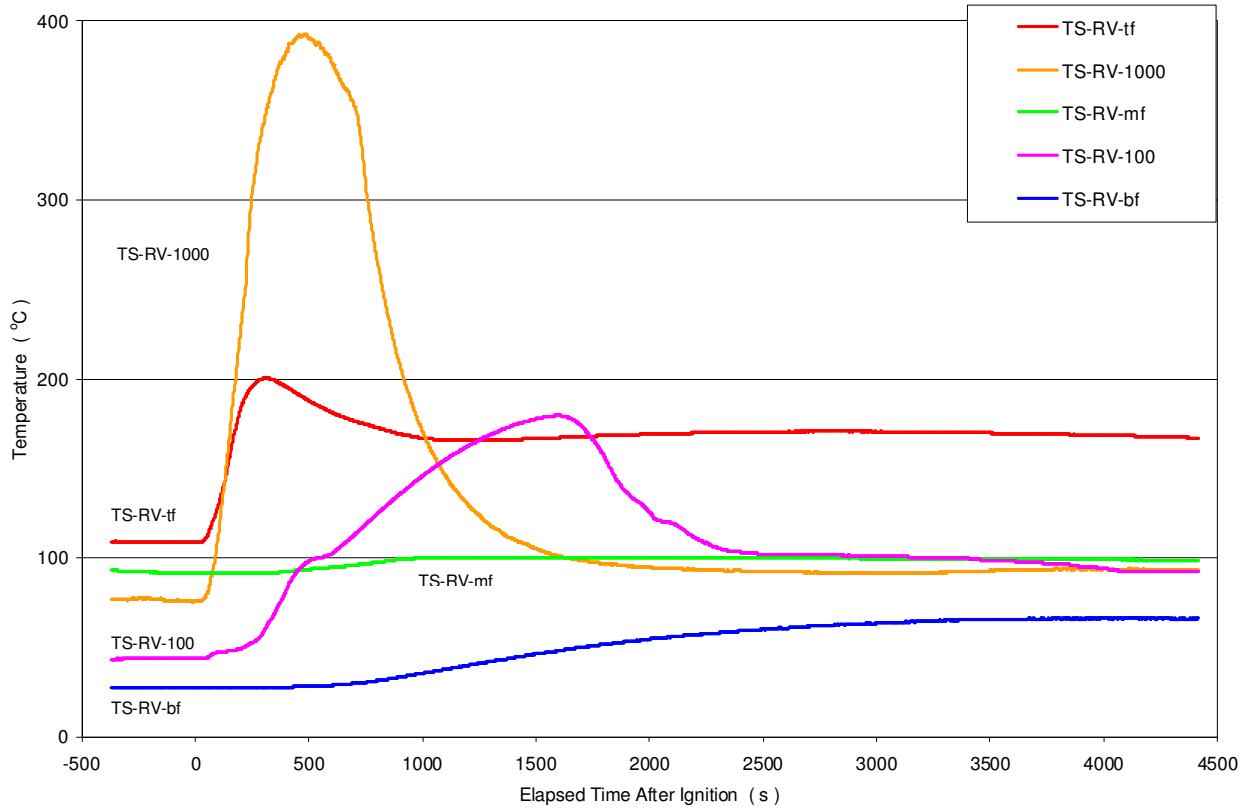

Figure A.5 Temperatures of selected steel structures.
Figure A.6 Total pressure in reaction vessel and position of valve V-quench.

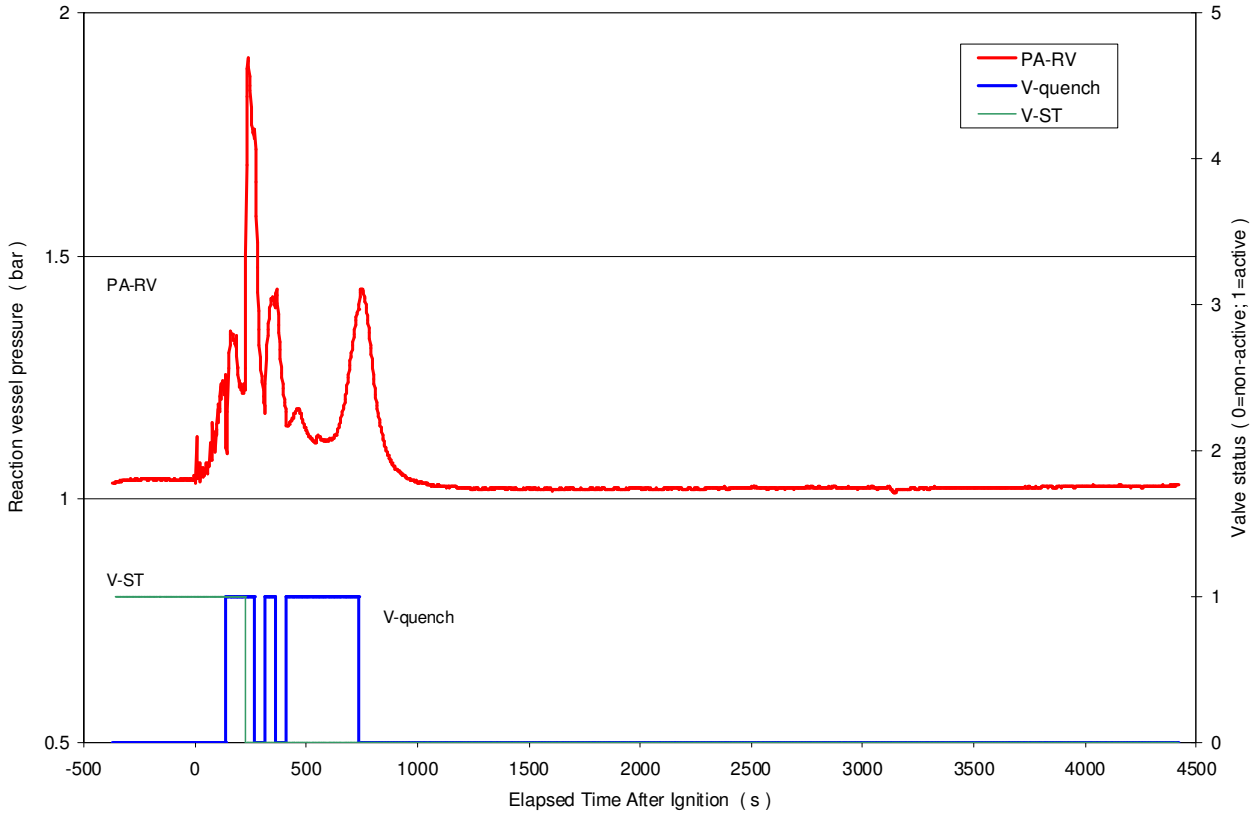

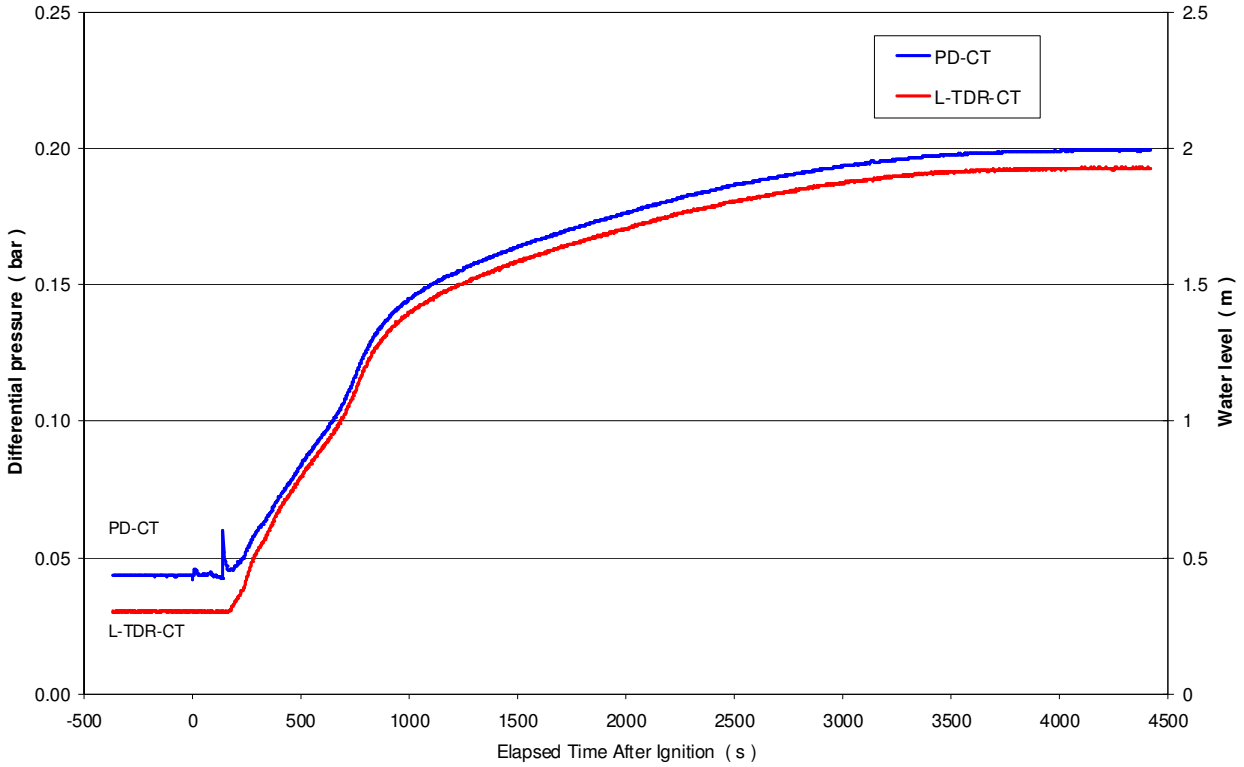

Figure A.7 Condensate tank inventory as measured by ΔP and level sensors.
Figure A.8 Condensate tank liquid inventory.

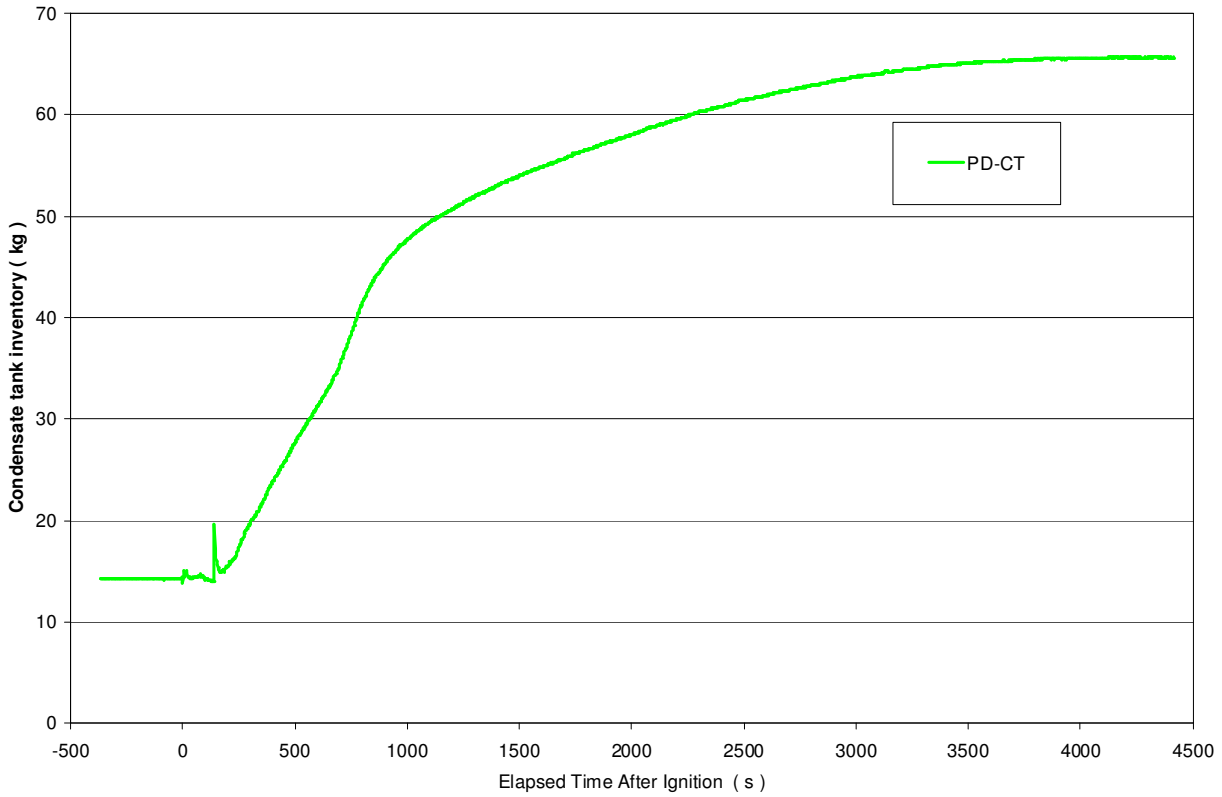

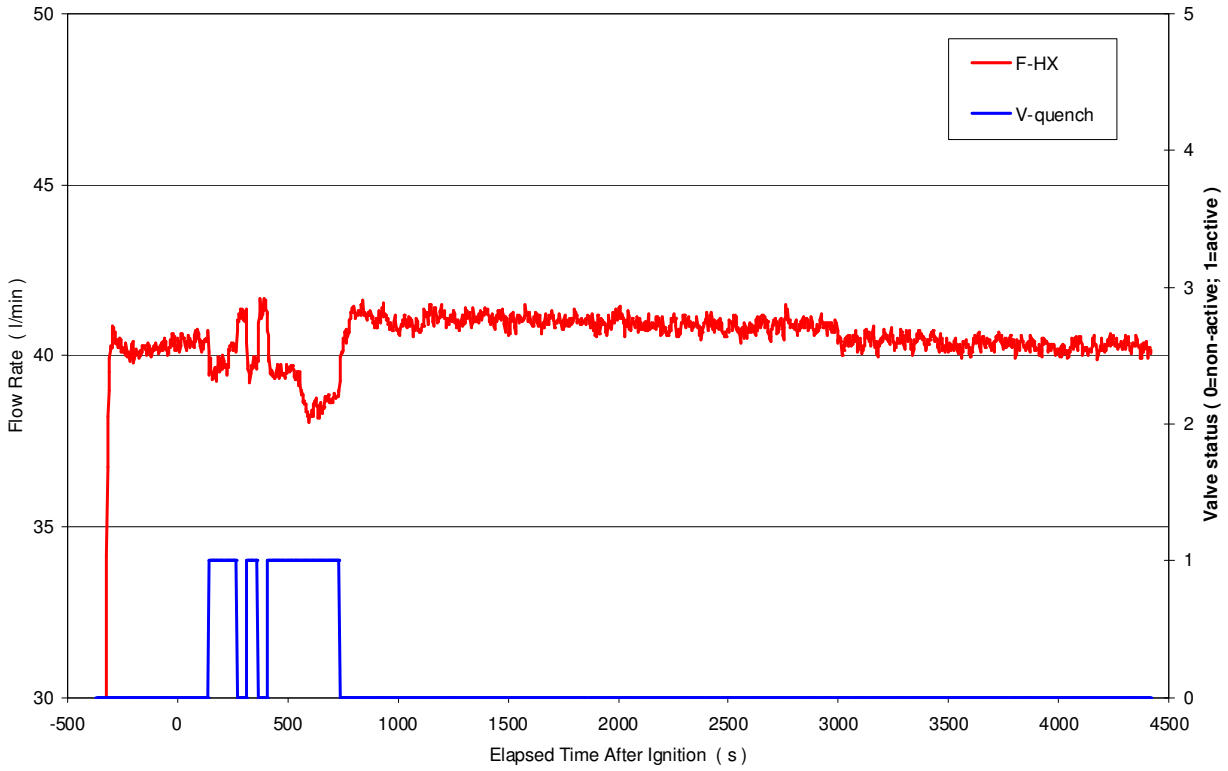

Figure A.9 HX secondary side flow rate and water injection valve position.
Figure A.10 Secondary side fluid temperatures at HX inlet and outlet.

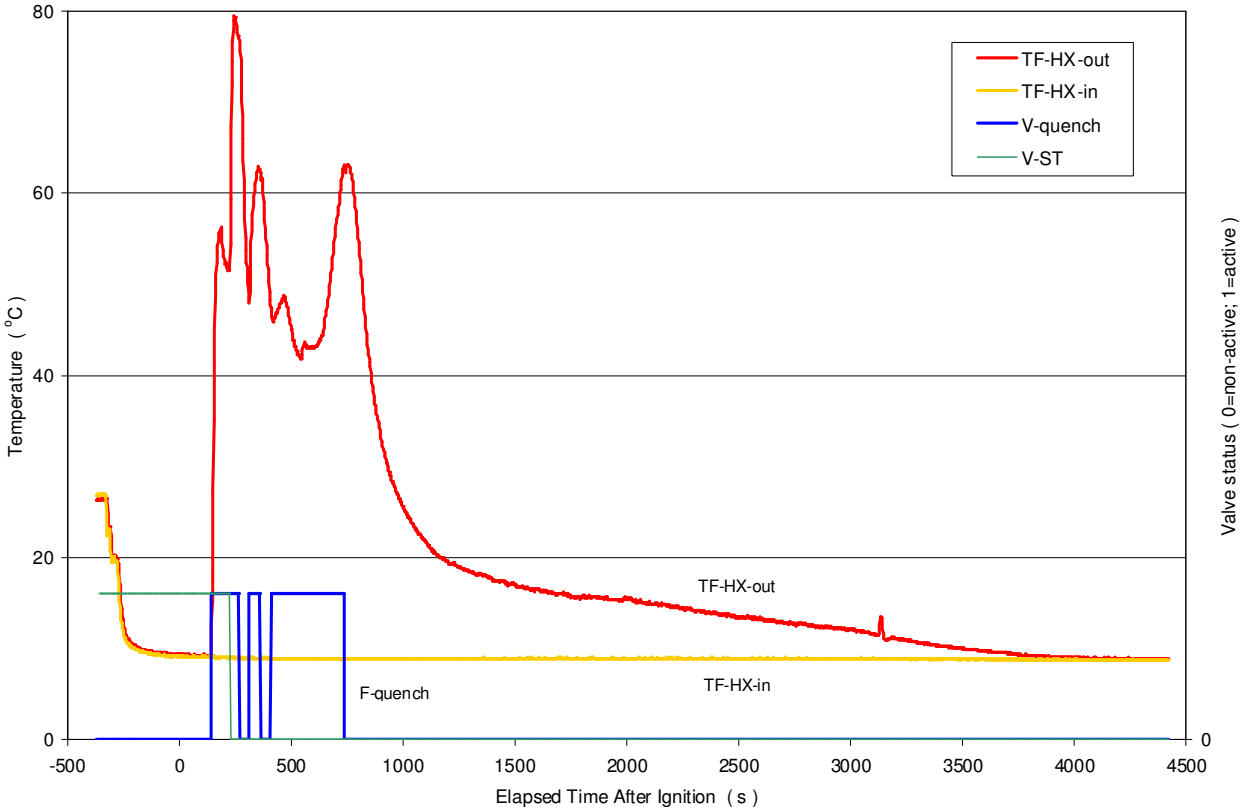

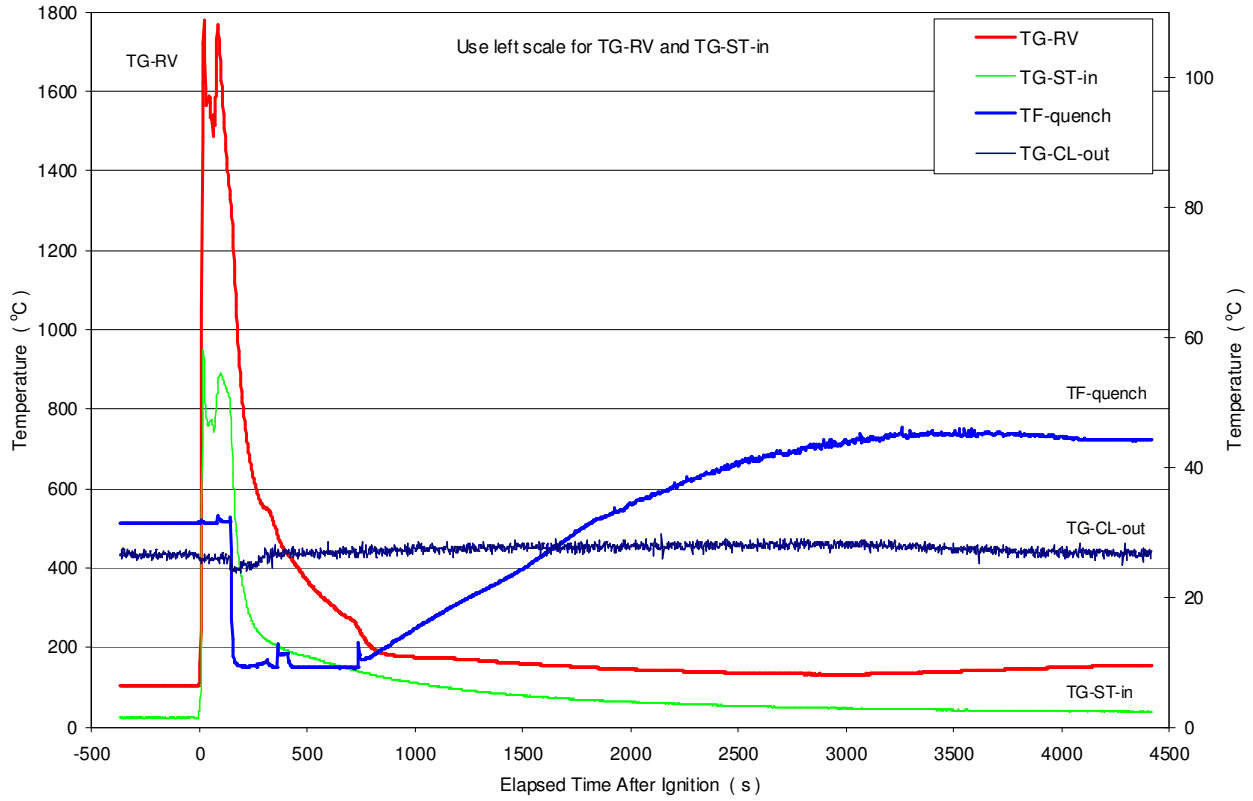

Figure A.11 Miscellaneous gas and fluid temperatures.
Figure A.12 Fluid temperatures in the condensate tank.

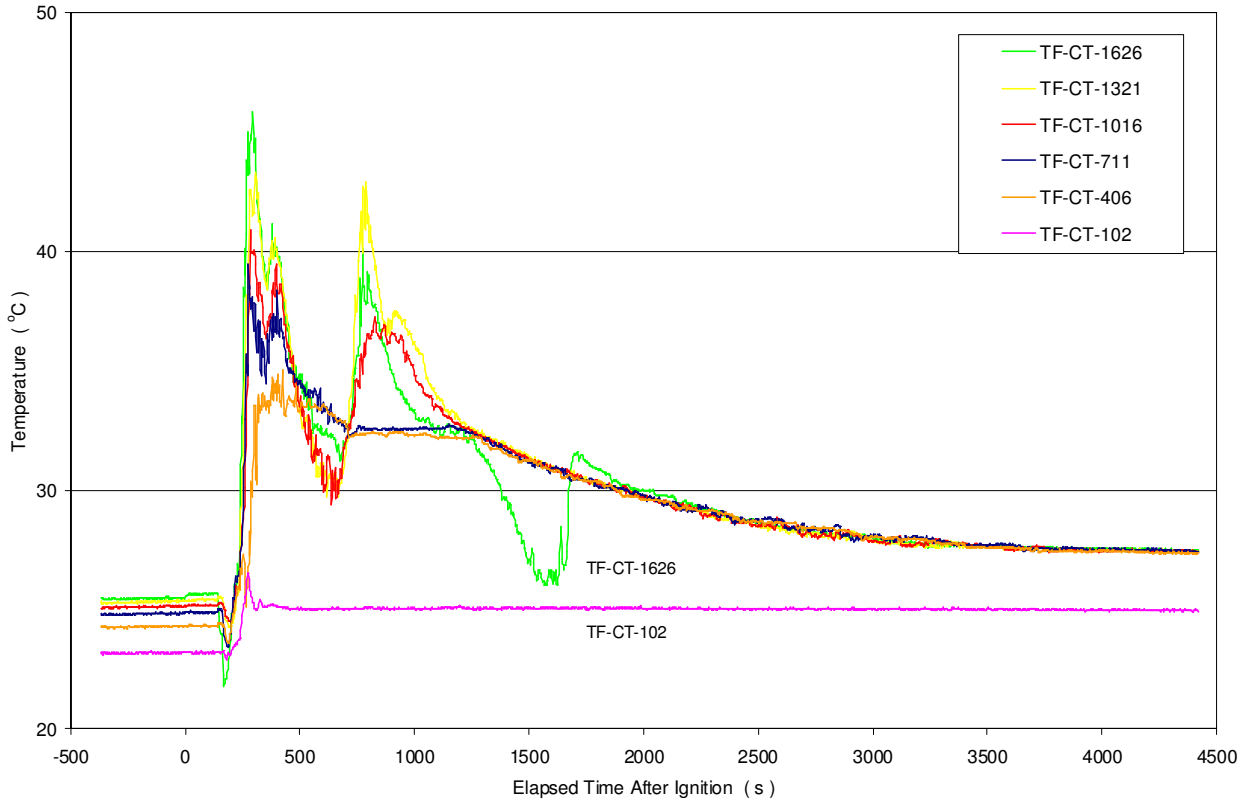

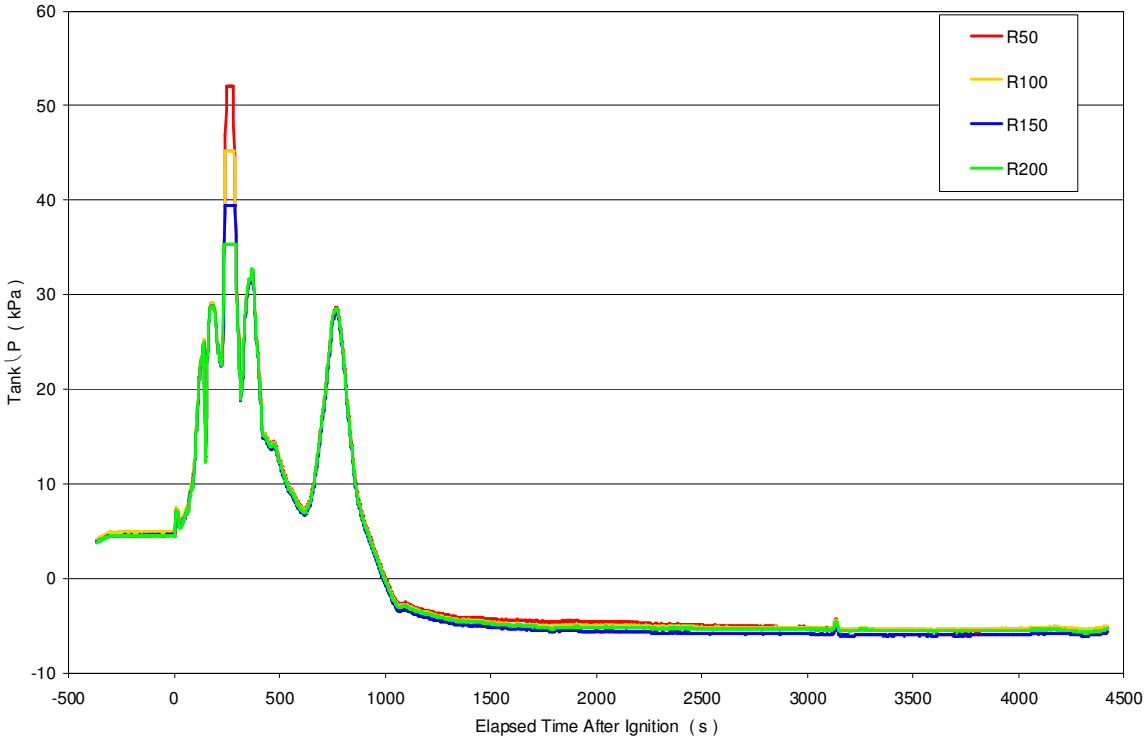
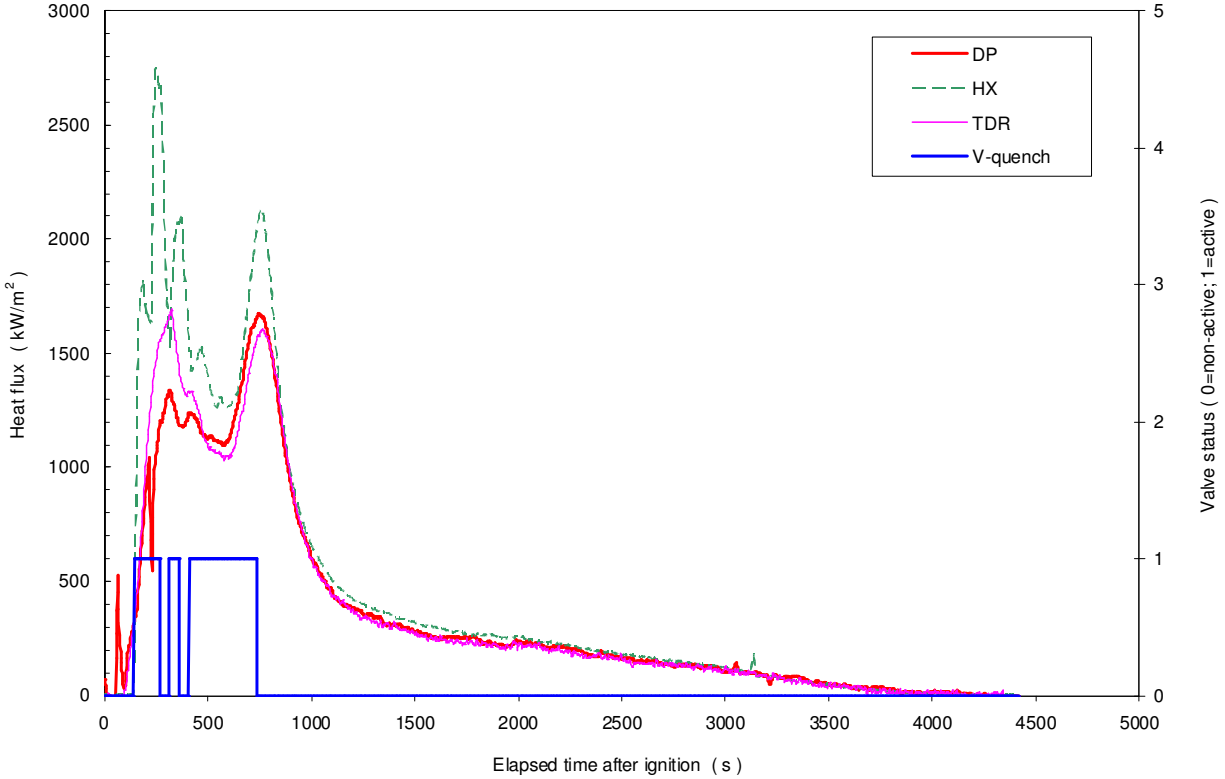
Figure A.13 Gauge pressure measured by reservoir level sensors.
Figure A.14 Heat flux as measured through condensate tank levels and HX heat load.